RMZ

MATERIALS and GEOENVIRONMENT

MATERIALI in GEOOKOLJE

RMZ – M&G, **Vol. 65**, No. 3
pp. 115–166 (2018)

Ljubljana, September 2018

RMZ – Materials and Geoenvironment
RMZ – Materiali in geookolje
ISSN 1408-7073

Old title/Star naslov
Mining and Metallurgy Quarterly/Rudarsko-metalurški zbornik
ISSN 0035-9645, 1952–1997

Published by/Izdajatelj
Faculty of Natural Sciences and Engineering, University of Ljubljana/
Naravoslovnotehniška fakulteta, Univerza v Ljubljani

Associated Publisher/Soizdajatelj
Institute for Mining, Geotechnology and Environment, Ljubljana/
Inštitut za rudarstvo, geotehnologijo in okolje
Velenje Coal Mine/Premogovnik Velenje
Slovenian Chamber of Engineers/Inženirska zbornica Slovenije

Editorial Office/Uredništvo
Technical editors/Tehnična urednika Teja Čeru and Jože Žarn
Secretary/Tajnica Nives Vukič

Editorial Address/Naslov uredništva
RMZ – Materials and Geoenvironment
Aškerčeva cesta 12, p. p. 312
1001 Ljubljana, Slovenija
Tel.: +386 (0)1 470 46 10
Fax.: +386 (0)1 470 45 60
E-mail: rmz-mg@ntf.uni-lj.si

Published/Izhajanje
4 issues per year/4 številke letno

Partly funded by Ministry of Education, Science and Sport of Republic of Slovenia./Pri financiranju revije sodeluje Ministrstvo za izobraževanje, znanost in šport Republike Slovenije.

Articles published in Journal "RMZ M&G" are indexed in international secondary periodicals and databases:/Članki, objavljeni v periodični publikaciji „RMZ M&G", so indeksirani v mednarodnih sekundarnih virih:
CA SEARCH® – Chemical Abstracts®, METADEX®, GeoRef.

Annual subscription for individuals in Slovenia: 20 EUR, for institutions: 30 EUR. Annual subscription for the rest of the world: 30 EUR, for institutions: 50 EUR/Letna naročnina za posameznike v Sloveniji: 20 EUR, za inštitucije: 30 EUR. Letna naročnina za tujino: 30 EUR, inštitucije: 50 EUR

Transaction account/Tekoči račun
Nova Ljubljanska banka, d. d., Ljubljana: UJP 01100-6030708186

VAT identification number/Davčna številka
24405388

Online Journal/Elektronska revija
www.rmz-mg.com
www.degruyter.com/view/j/rmzmag

Table of Contents

Kazalo

Historical Review

More than 90 years have passed since the University Ljubljana in Slovenia was founded in 1919. Technical fields were united in the School of Engineering that included the Geologic and Mining Division, while the Metallurgy Division was established only in 1939. Today, the Departments of Geology, Mining and Geotechnology, Materials and Metallurgy are all part of the Faculty of Natural Sciences and Engineering, University of Ljubljana.

Before World War II, the members of the Mining Section together with the Association of Yugoslav Mining and Metallurgy Engineers began to publish the summaries of their research and studies in their technical periodical Rudarski zbornik (Mining Proceedings). Three volumes of Rudarski zbornik (1937, 1938 and 1939) were published. The War interrupted the publication and it was not until 1952 that the first issue of the new journal Rudarsko-metalurški zbornik – RMZ (Mining and Metallurgy Quarterly) was published by the Division of Mining and Metallurgy, University of Ljubljana. Today, the journal is regularly published quarterly. RMZ – M&G is co-issued and co-financed by the Faculty of Natural Sciences and Engineering Ljubljana, the Institute for Mining, Geotechnology and Environment Ljubljana, and the Velenje Coal Mine. In addition, it is partly funded by the Ministry of Education, Science and Sport of Slovenia.

During the meeting of the Advisory and the Editorial Board on May 22, 1998, Rudarsko-metalurški zbornik was renamed into "RMZ – Materials and Geoenvironment (RMZ – Materiali in Geookolje)" or shortly RMZ – M&G. RMZ – M&G is managed by an advisory and international editorial board and is exchanged with other world-known periodicals. All the papers submitted to the RMZ – M&G undergoes the course of the peer-review process.

RMZ – M&G is the only scientific and professional periodical in Slovenia which has been published in the same form for 60 years. It incorporates the scientific and professional topics on geology, mining, geotechnology, materials and metallurgy. In the year 2013, the Editorial Board decided to modernize the journal's format.

A wide range of topics on geosciences are welcome to be published in the RMZ – Materials and Geoenvironment. Research results in geology, hydrogeology, mining, geotechnology, materials, metallurgy, natural and anthropogenic pollution of environment, biogeochemistry are the proposed fields of work which the journal will handle.

Editor-in-Chief

Zgodovinski pregled

Že več kot 90 let je minilo od ustanovitve Univerze v Ljubljani leta 1919. Tehnične stroke so se združile v Tehniški visoki šoli, ki sta jo sestavljala oddelka za geologijo in rudarstvo, medtem ko je bil oddelek za metalurgijo ustanovljen leta 1939. Danes oddelki za geologijo, rudarstvo in geotehnologijo ter materiale in metalurgijo delujejo v sklopu Naravoslovnotehniške fakultete Univerze v Ljubljani.

Pred 2. svetovno vojno so člani rudarske sekcije skupaj z Združenjem jugoslovanskih inženirjev rudarstva in metalurgije začeli izdajanje povzetkov njihovega raziskovalnega dela v Rudarskem zborniku. Izšli so trije letniki zbornika (1937, 1938 in 1939). Vojna je prekinila izdajanje zbornika vse do leta 1952, ko je izšel prvi letnik nove revije Rudarsko-metalurški zbornik – RMZ v izdaji odsekov za rudarstvo in metalurgijo Univerze v Ljubljani. Danes revija izhaja štirikrat letno. RMZ – M&G izdajajo in financirajo Naravoslovnotehniška fakulteta v Ljubljani, Inštitut za rudarstvo, geotehnologijo in okolje ter Premogovnik Velenje. Prav tako izdajo revije financira Ministrstvo za izobraževanje, znanost in šport.

Na seji izdajateljskega sveta in uredniškega odbora je bilo 22. maja 1998 sklenjeno, da se Rudarsko-metalurški zbornik preimenuje v RMZ – Materiali in geookolje (RMZ – Materials and Geoenvironment) ali skrajšano RMZ – M&G. Revijo RMZ – M&G upravljata izdajateljski svet in mednarodni uredniški odbor. Revija je vključena v mednarodno izmenjavo svetovno znanih publikacij. Vsi članki so podvrženi recenzijskemu postopku.

RMZ – M&G je edina strokovno-znanstvena revija v Sloveniji, ki izhaja v nespremenjeni obliki že 60 let. Združuje področja geologije, rudarstva, geotehnologije, materialov in metalurgije. Uredniški odbor je leta 2013 sklenil, da posodobi obliko revije.

Za objavo v reviji RMZ – Materiali in geookolje so dobrodošli tudi prispevki s širokega področja geoznanosti, kot so: geologija, hidrologija, rudarstvo, geotehnologija, materiali, metalurgija, onesnaževanje okolja in biokemija.

Glavni urednik

Original scientific paper

Received: May 01, 2018
Accepted: Jun 08, 2018
DOI 10.2478/rmzmag-2018-0014

Determination of Emissivity of Brass Alloy using Infrared Thermographic Technique

Določitev emisivnosti medi z uporabo infrardeče termografije

Zorana Lanc*, Milan Zeljković, Aleksandar Živković, Branko Štrbac, Miodrag Hadžistević
Faculty of Technical Sciences, University of Novi Sad, Serbia
* zoranalanc@uns.ac.rs

Abstract

This paper presents the experimental determination of the dependence of emissivity of brass on surface roughness and temperature. The investigation was conducted using the infrared thermographic technique on brass alloy C27200 workpieces with different degrees of surface roughness, during the continuous cooling process. The results obtained showed that the emissivity of the chosen brass alloy increases with greater surface roughness and decreases during the cooling process, its value ranging from 0.07 to 0.19. It was concluded that surface roughness has a greater influence on the increase of the emissivity at higher temperatures, which can be seen in the three-dimensional infrared images. Multiple regression analysis confirmed a strong correlation between the examined parameters and the emissivity, and an original multiple regression model was determined.

Key words: emissivity, brass, infrared thermographic technique (ITT), three-dimensional infrared (3D IR) images, regression analysis.

Povzetek

V prispevku je prikazano eksperimentalno določanje emisivnosti medi glede na hrapavost in temperaturo površine. Izvedena je bila raziskava na obdelovancih iz medi C27200 z različnimi stopnjami hrapavosti površine med postopkom neprekinjenega hlajenja in z uporabo infrardeče termografije (ITT). Dobljeni rezultati so pokazali, da se emisivnost preizkušane medi povečа z večjo površinsko hrapavostjo in se med procesom hlajenja zmanjša, njena vrednost pa se giblje med 0,07 in 0,19. Pri višjih temperaturah ima hrapavost večji vpliv na povečanje emisivnosti, kar je razvidno na tridimenzionalnih infrardečih slikah (3D IR). Večkratna regresijska analiza je potrdila močno korelacijo med preiskovanimi parametri in emisivnostjo. Določen je bil izvirni večkratni regresijski model.

Ključne besede: emisivnost, med, infrardeča termografija (ITT), tridimenzionalne infrardeče slike (3D IR), regresijska analiza.

Introduction

Infrared thermographic technique (ITT) is one of the non-destructive testing techniques used for preventive and predictive maintenance, as well as for non-contact temperature measurement [1,2]. ITT works on the principle of transformation of spatial variations in the infrared (IR) radiation emitted from the surface of an observed object into a two-dimensional (2D) IR image, where the differences in temperature distribution are presented as a range of colours or tones [3]. The key material parameter for the practical use of ITT is emissivity. Emissivity is defined as the ratio of emissive power of the materials' surface (grey body) to that of an ideal black body under the same geometric and spectral conditions [4]. The emissivity of a metal can easily change due to physical and chemical conditions of the surface, such as the type of material, surface roughness, microstructure, temperature, wavelength, and so on [5]. Due to the low and varying emissivity of metals, numerous authors have investigated the effect of these mentioned parameters on metals' emissivity characteristics. Deheng et al. [6] studied the effect of surface oxidation on the spectral emissivity of brass over the temperature range from 527°C to 797°C at the wavelength of 1.5 μm. The temperature of the specimen surface is monitored by averaging the two R-type platinum–rhodium thermocouples. It was shown that the spectral emissivity of brass rapidly increases with increasing temperature [6]. Zhibin et al. [7] investigated the influence of the surface roughness on the emissivity of the Au films for high-temperature application. The samples were heated in air at 600°C for 200 h to simulate the application environment. The results showed that the substrate roughness had great influence on the emissivity characteristics of the Au films. The average IR emissivity of the samples with low roughness just increased a little after heat treatment, while it greatly increased for the sample with high roughness [7]. Wen and Mudawar [8] determined the emissivity of different aluminium alloys depending on temperature, surface roughness and oxidation, using multispectral radiation thermometry. At the same temperature, the emission spectra of different alloys were similar in shape, but oxidation led to significant differences in the magnitude. An increase in temperature and surface roughness mostly resulted in higher emissivity of the examined alloys [9, 10].

Previous studies showed that the emissivity of metals increases with increase in temperature and surface roughness during heating. This paper includes an investigation into the emissivity behaviour of the brass alloy C27200 during the continuous cooling process when using ITT. The reason for this is the similar heating and cooling rates of metals. For a more detailed analysis of the effect of surface roughness and temperature on the emissivity characteristics of brass alloy C27200, three-dimensional IR images (3D IR) were used. This study considered the possibility of use of multiple regression analysis for the theoretical determination of the emissivity, on the basis of experimentally obtained data. The aim of the study was to investigate whether ITT can be used for reliable temperature measurement of heated metal surfaces on the work equipment and, by implication, for the assessment of risk of burn injuries.

Materials and methods

The experimental determination of the emissivity was conducted on the brass alloy C27200. Due to the excellent mechanical properties, machinability and corrosion resistance of brass, it is widely used in pipes, valves and fittings in systems that transport water and other aqueous fluids [11]. Chemical characteristics of the chosen brass alloy are given in Table 1.

Table 1. *Chemical characteristics of the chosen brass alloy*

UNS No.	ISO No.	Common name	Copper %	Zinc %
C27200	CuZn37	63/37 Common brass	62–65	~37

For the purpose of the experimental work, four workpieces were made with dimensions of (150 × 150 × 10) mm. The first workpiece was ground, whereas the other three were milled under different regimes of face milling with the

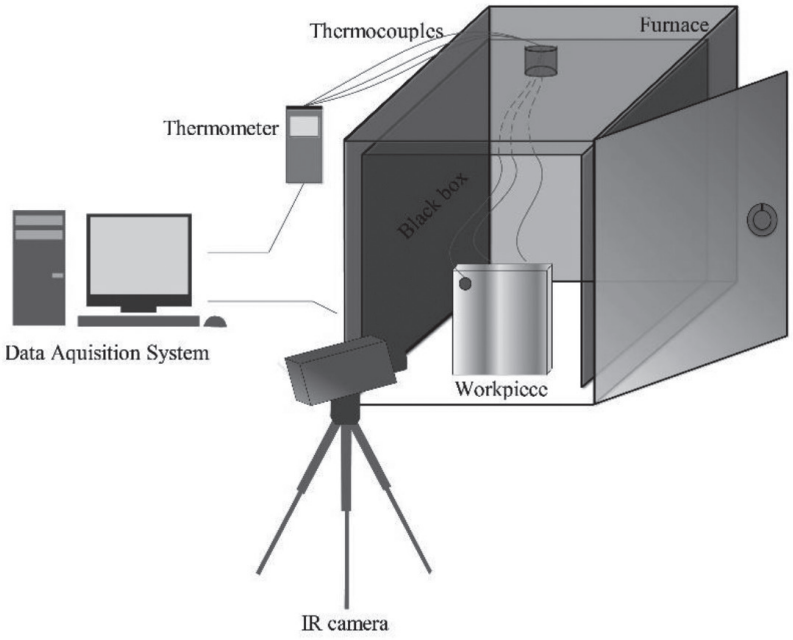

Figure 1. *Experimental set-up.*

Table 2. *Surface roughness of the workpieces*

Type of machining	Roughness average, $\overline{Ra}$ [µm]	Labels
Grinding	1.23	B_1
Milling	3.24	B_2
	3.38	B_3
	3.92	B_4

aim of obtaining different surface qualities, i.e., roughness values. The roughness of the workpieces was measured with a contact method using a Mar Surf PS1 device. The mean roughness (roughness average, *R*a) was measured at 30 points uniformly distributed on the surface of the workpiece. The average value of the measured roughness (*Ra*) was taken as the surface roughness of the workpiece (Table 2).

A common method for determining the emissivity using an IR camera is based on the simultaneous heating of a workpiece, measuring the temperature using an IR camera and measuring the reference temperature on the analysed surface. The reference temperature can be measured using a contact device for temperature measurement or by applying a special coating with known emissivity on the examined surface within the field of view of the IR camera. The emissivity is determined by adjusting the value from zero to one until the temperatures on the IR camera and the reference temperature are equal [12]. For the purpose of this paper, a heat treatment furnace was used for heating the workpieces. For achieving a uniform temperature distribution on the target area of the sample, every workpiece was placed upright in the centre of the furnace and tested separately. The radiation emitted from the heat furnace can affect the thermography test to a large extent. Thus, prior to the measurement, a 2-mm black tin box was placed into the furnace in order to eliminate the effect of the furnace walls on the measurement results. The IR camera used for thermal imaging was camera IR ThermoPro TP8S, with a spectral range of 8–14 µm and temperature accuracy of ±1°C. The reference temperature was measured using type-K thermocouples. Two thermocouples were placed on the back surface of the workpiece, whereas the third thermocouple was attached to the front surface of the workpiece using black rubber. The experimental set-up is presented in Figure 1.

After installing the thermocouples and setting the IR camera, a workpiece was heated up to 200°C. On reaching this temperature, the work-

piece was cooled down to the ambient temperature of 25°C. At the same time, the camera took an IR image of the workpiece at every 10°C decrease in temperature. The described procedure was repeated for every workpiece. The obtained IR images were processed using the Guide Ir Analyser program, where the average emissivity of a workpiece was adjusted to a value ranging from zero to one until the temperature became equal to the reference temperature. During the IR-image processing step, the temperature used as the reference temperature was the average of the temperature values obtained with the thermocouples. The described method was used for determining the emissivity of all four workpieces at temperatures ranging from 50°C to 200°C.

Results and discussion

The experimental data show that the average emissivity of brass alloy C27200 in the spectral range of 8–14 μm decreases during the cooling and mainly increases with an increase in the surface roughness (Figure 2). The emissivity ranges from 0.07 to 0.19. At temperatures from 50°C to 120°C, the emissivity values of the workpieces are constant, and their mutual differences are only the results of the surface roughness. At temperatures >120°C, the emissivity values increase, first with the B_3 workpiece and finally with the B_4 workpiece. The emissivity of the ground workpiece B_1 is the lowest and not prone to drastic changes as in the case of the other workpieces, which were milled.

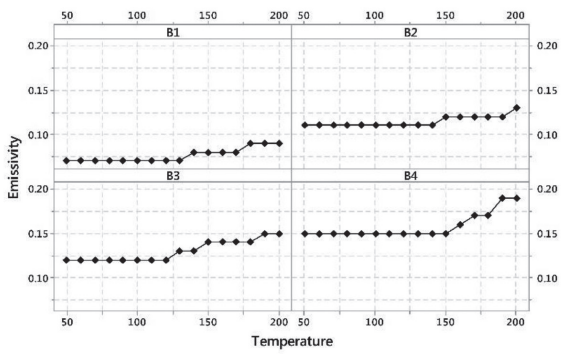

Figure 2. *Emissivity of brass alloy C27200 at low and medium temperatures.*

Study of 3D IR images

A more thorough investigation into the effects of the temperature and surface roughness on the emissivity was conducted using 3D IR images. 3D IR images are the three-dimensional representations of the surface of a workpiece, with more strictly defined boundaries between the areas with small temperature differences, which are almost invisible in a normal IR image. There are various commercial software programs for the construction of 3D IR images, but in this paper, we used the new method presented by Lanc et al. [13]. The method is based on exporting the temperature values per pixel of an IR image using the Guide Ir Analyser program into a Microsoft Excel table. In the table, the data are grouped in such a way that the *x*- and *y*-coordinates determine the position of a pixel in the IR image, whereas the *z*-coordinate determines its temperature. With a simple selection of all the data and the construction of a surface contour diagram in Microsoft Excel, 3D IR images are obtained. Figure 3 presents the 3D IR images of the ground workpiece B_1 and the workpiece with the greatest surface roughness, B_4, at the temperature of 50°C.

Their comparison shows that the temperature is more evenly distributed in the B_4 workpiece than in the B_1 workpiece due to the more reflective surface of the B_1 workpiece. While measuring the arithmetic mean roughness using the Mar Surf PS1 device, it was noticed that the right side of the B_4 workpiece had a greater roughness than the left side. These data correspond to the presented 3D IR images of the B_4 workpieces. Although the average temperature of both workpieces was 200°C, in the B_4 workpiece, temperatures from 0°C to 50°C were more frequent than in the B_1 workpiece, where the most frequent temperatures ranged from 50°C to 100°C. The reflective surface contributed to the higher temperature of the B_1 workpiece. The defects are clearly visible in Figure 4 and are represented with yellow areas, which correspond to the highest temperatures. In Figure 4, the temperature of black rubber is >400°C, although its real temperature is 200°C. This error occurred because it is possible to adjust only one value of the emissivity in a 3D IR image. In this case, the values of the emissivity were adjusted for the B_1 and B_4 workpieces,

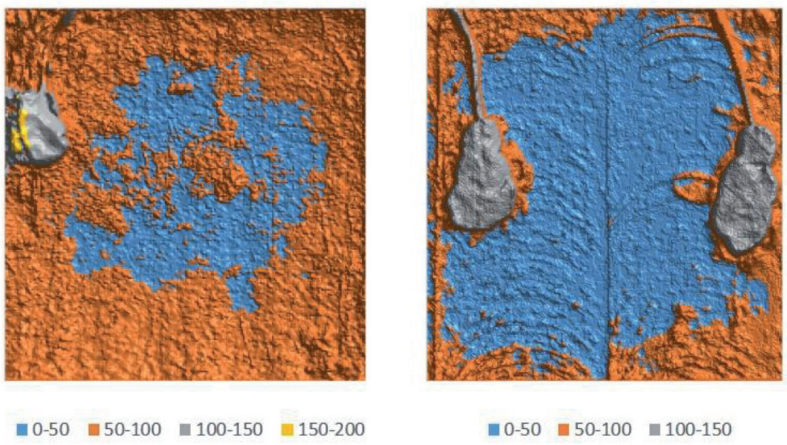

Figure 3. *3D IR images of B_1 workpiece (left) and B_4 workpiece (right) at the temperature of 50°C.*

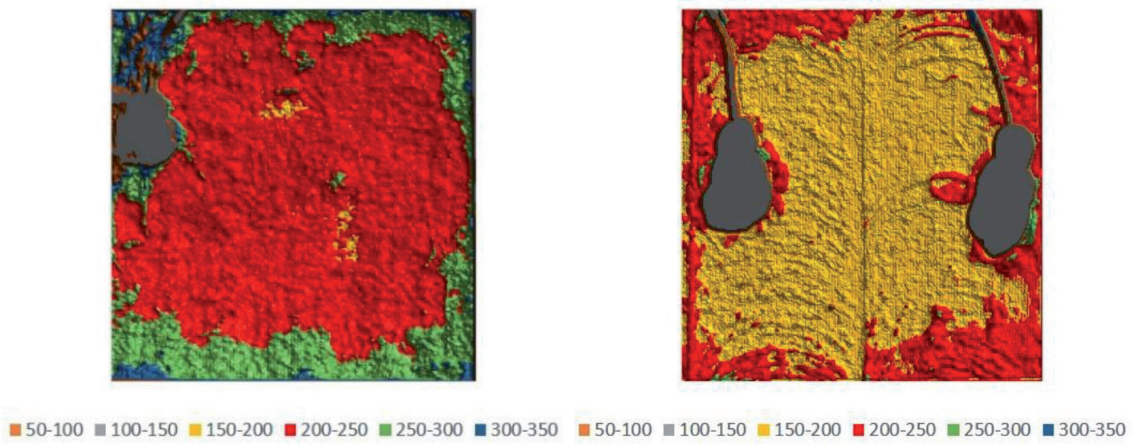

Figure 4. *3D IR images of B_1 workpiece (left) and B_4 workpiece (right) at the temperature of 200°C.*

which is why the temperatures of black rubber drastically increased.

The effect of the reflected radiation on the bottom part of the workpiece is noticeable here as well, leading to the so-called 'false temperatures'. At higher temperatures, the differences in the surface roughness are more conspicuous than at lower temperatures. In the 3D IR images of the milled workpieces, the difference in the surface roughness is bigger at the temperature of 200°C than at the temperature of 50°C. At higher temperatures, the milling direction and the boundaries between the tool passes are more conspicuous, which can be seen in the 3D IR images of the B_4 workpiece, whose surface was machined in two tool passes. This leads to a conclusion that the surface roughness causes a greater increase in the emissivity at higher temperatures.

Multiple linear regression analysis

Multiple regression analysis makes it possible to examine the effect of several independent variables on the dependent output variable. The result of this approach is a multiple regression model, which, in the form of a mathematical formula, connects the effect of two independent variables on the dependent variable [14]. In this concrete case, the dependent variable – the emissivity (ε) – is related to two independent variables – temperature (T) and surface roughness (R_a) – according to the following model (Equation 1):

$$\varepsilon = \beta_0 + \beta_1 \cdot T + \beta_2 \cdot Ra + r \qquad (1)$$

where $\beta_0, \beta_1, \beta_2, \beta_0$ represent the regression coefficients and r is the component of random error.

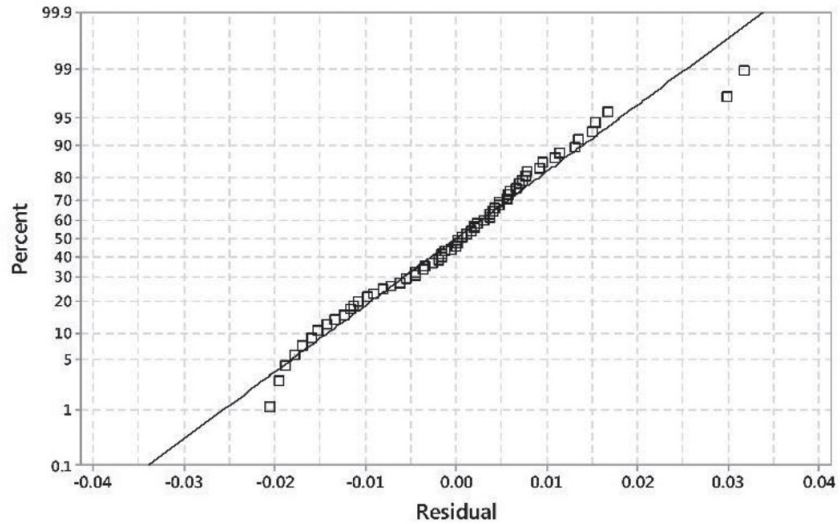

Figure 5. *Scatter plot.*

For assessment of the model for $n = 64$ observations and the number of independent variables $k = 2$, the matrix form of Equation 1 is given by the following matrix Equation 2:

$$Y = \begin{bmatrix} e_1 \\ e_2 \\ \vdots \\ e_{64} \end{bmatrix}; \; X = \begin{bmatrix} 1 & x_{11} & x_{12} \\ 1 & x_{21} & x_{22} \\ \vdots & \vdots & \vdots \\ 1 & x_{(64)1} & x_{(64)2} \end{bmatrix}; \tag{2}$$

$$\beta = \begin{bmatrix} \beta_0 \\ \beta_1 \\ \beta_2 \end{bmatrix}; \; \beta = \begin{bmatrix} r_0 \\ r_1 \\ \vdots \\ r_{64} \end{bmatrix}.$$

The matrix Equation 2 is solved according to results in the following multiple linear regression model (Equation 3):

$$\varepsilon = 0.000179 \cdot T + 0.027565 \cdot Ra - 0.06101 \tag{3}$$

The presented model can be used for the temperature range from 50°C to 200°C and surface roughness ranging from 1.23 μm to 3.92 μm. In this case, the multiple coefficient of determination R^2 shows that 87.94% of the variation in the emissivity comes from variation in the temperature and surface roughness, whereas the remaining 13.06% is the consequence of the effect of other parameters, such as humidity, permeability of the atmosphere, temperature of the environment, and so on. The model can be used for prediction of the emissivity at temperatures and surface roughness values that are beyond the mentioned ranges, with a somewhat lower coefficient of determination R^2_{pred} of 87.55%. Multiple regression was used to determine the strength of dependence between the emissivity and the observed parameters based on the correlation coefficient r. The correlation coefficient was 0.9, which points to the fact that there is a strong (direct) linear dependence between temperature and surface roughness on the one hand and the emissivity on the other hand. The scatter plot (Figure 5) shows a small degree of data deviation around the established regression line, indicated by the value of the standard error S of 0.01.

Conclusions

The emissivity of brass alloy C27200 during the process of cooling from 200°C to 50°C was experimentally determined using the ITT.

The investigation showed that the emissivity of the chosen alloy ranges from 0.07 to 0.19 and that it decreases with decrease in temperature and increases with increase in surface roughness. At higher temperatures, the differences between the emissivity values of the workpieces are bigger. The analysis of 3D IR images showed that this phenomenon is a consequence of a more significant effect of surface roughness on the emissivity at higher temperatures.

Additionally, the paper used a new method of creating 3D IR images using Microsoft Excel. This method is simple, and unlike commercial programs, it is more affordable. Although ITT is not recommendable for the precise determination of the emissivity of metals, in the post-processing stage of IR images, the authors managed to determine small variations in the emissivity, even when the differences between the IR images were 10°C. Multiple regression analysis confirmed a strong correlation between the investigated parameters and the emissivity, and a multiple regression model was determined.

The herein-presented model can only be applied with low and medium temperatures, since at higher temperatures, there is a somewhat greater deviation of the experimental data from the regression line. The reason for this is the uneven distribution of temperature on the surface of a workpiece due to the defects that occur during its machining.

References

[1] Krešák, J., Peterka, P., Kropuch, S., Novák, L. (2014): Measurement of tight in steel ropes by a mean of thermovision, *Measurement*, 50, pp. 93–98.

[2] Kosec, B., Karpe, B., Budak, I., Ličen, M., Đorđević, M., Nagode, A., Kosec, G. (2012): Efficiency and quality of inductive heating and quenching of planetary shafts, *Metallurgy*, 51, pp. 71–74.

[3] Glavaš, H., Jozsa, L., Barić, T. (2016): Infrared thermography in energy audit of electrical installations, *Tehnički vjesnik*, 23, pp. 1533–1539.

[4] HangJin, J., Jonathan, K., Kyle, B., Kumar, S. (2017): Spectral emissivity of oxidized and roughened metal surfaces. *International Journal of Heat and Mass Transfer*, 115, Part B, pp. 1065–1071.

[5] Švantner, M., Honnerová, P., Veselý, Z. (2016): The influence of furnace wall emissivity on steel charge heating. *Infrared Physics & Technology*, 74, pp. 63–71.

[6] Deheng, S., Qionglan, L., Zunlue, Z., Jinfeng, S., Baokui, W. (2014): Experimental study of the relationships between the spectral emissivity of brass and the temperature in the oxidizing environment. *Infrared Physics & Technology*, 64, pp. 119–124.

[7] Zhibin, H., Wancheng, Z., Xiufeng, T., Dongmei, Z., Fa, L. (2011): Effects of substrate roughness on infrared-emissivity characteristics of Au films deposited on Ni alloy. *Thin Solid Films*, 519, pp. 3100–3106.

[8] Wen, C.D., Mudawar, I. (2004): Emissivity characteristics of roughened aluminum alloy surfaces and assessment of multispectral radiation thermometry (MRT) emissivity models. *International Journal of Heat and Mass Transfer*, 47, pp. 3591–3605.

[9] Kosec, B., Kosec, G. (2003): Temperature field analysis on active working surface of the die-casting die. *Metall*, 57, pp. 134–136.

[10] Wen, C.D., Mudawar, I. (2006): Modeling the effects of surface roughness on the emissivity of aluminum alloys. *International Journal of Heat and Mass Transfer*, 49, pp. 4279–4289.

[11] Yang, C., Ding, Z., Tao, Q.C., Liang, L., Ding, Y.F., Zhang, W.W., Zhu, Q.L. (2018): High-strength and free-cutting silicon brass alloy C27200es designed via the zinc equivalent rule. *Materials Science and Engineering*, 723, pp. 296–305.

[12] Švantner, M., Vacíková, P., Honner, M. (2013): Non-contact charge temperature measurement on industrial continuous furnaces and steel charge emissivity analysis. *Infrared Physics & Technology*, 61, pp. 20–26. doi: 10.1016/j.infrared.2013.07.005.

[13] Lanc, Z., Štrbac, B., Zeljković, M., Živković, A., Hadžistević, M. (2018): Emissivity of Aluminium Alloy using Infrared Thermographic Technique. *Materials and Technology*, 52, pp. 35–40.

[14] Motorcu, A.R., Isik, Y., Kus, A., Cakir, M.C. (2016): Analysis of the cutting temperature and surface roughness during the orthogonal machining of AISI 4140 alloy steel via the Taguchi method, Materials and technology, 50(3), 343–351. doi:10.17222/mit.2015.021.

Original scientific paper

Received: November 30, 2017
Accepted: May 17, 2018
DOI: 10.2478/rmzmag-2018-0013

Assessment of the influences of climate variability on nitrogen leaching rate into groundwater

Ocena vplivov podnebne spremenljivosti na stopnjo izpiranja dušika v podzemno vodo

Sara Uhan[1,*]
[1] Polje Cesta XVI/19, SI-1260 Ljubljana Polje, Slovenija
* sara.uhan@gmail.com

Abstract

This article presents preliminary model results of climate change impact on biogeochemical processes in soil. With the use of DNDC (DeNitrification-DeComposition) model, a simulation with climate data over seventy years period (1947–2016) from central part of Slovenia has been carried out. Amongst assessed sources of variability, time variability has been estimated to around 10% of the total annual nitrogen leaching. In some cases, a statistically significant downward trend was observed with a 5 kg reduction in nitrogen per hectare in seventy years period. This study represents the first quantitative assessment of nitrogen leaching variability due to precipitation and air temperature variability in three representative soil profiles in the central Slovenia. It offers a starting point for future regional research for the purpose of farming practice optimization, especially in catchment areas of major regional water resources in Slovenia.

Key words: climate variability, denitrification, nitrogen leaching

Izvleček

Članek predstavlja preliminarne rezultate modeliranja vpliva klimatske spremenljivosti na biogeokemične procese v tleh. Na simulacijah z modelom DNDC (DeNitrification-DeComposition) so bili v sedemdeset--letnem obdobju (1947–2016) za osrednjo Slovenijo ocenjeni posamezni viri variabilnosti letne količine izpranega dušika, med katerimi zavzema časovna spremenljivost okoli 10%. V nekaterih primerih je bil ugotovljen statistično značilen trend zniževanja s 5 kilogramskim zmanjšanjem dušika na hektar v sedemdesetletnem obdobju. Študija predstavlja prvo kvantitativno oceno spremembe izpiranja dušika v treh reprezentativnih profilih tal v osrednjem delu Slovenije zaradi spremenljivosti padavin in temperature zraka ter ponuja izhodišče nadaljnjim regionalnim raziskavam za potrebe optimizacije kmetijske prakse, predvsem na prispevnih območjih pomembnih regionalnih vodnih virov v Sloveniji.

Ključne besede: podnebna spremenljivost, denitrifikacija, izpiranje dušika

Introduction

Groundwater is a dominant source of public water supply in Slovenia [1]; the inalienable right to drinking water is also enshrined in the Constitution of the Republic of Slovenia [2]. With this definition, our society has accepted responsibility and a clear commitment to preserve natural water resources for the sustainable water supply. The quantitative status of all groundwater bodies in Slovenia is assessed as good with the share of yearly pumped water quantity being only 3,1% of long-term available groundwater quantities [3]. Groundwater chemical status, however, has been assessed as poor in three groundwater bodies, mainly due to exceeding nitrate threshold value [4]. Groundwater quantities in water bodies with poor chemical status exceed quantities of yearly pumped groundwater in the country. Knowing the variability of the effects of individual processes in the nitrogen cycle is therefore crucial for the planning of measures to reduce nitrate pollution, with a simultaneous need for sustainable agriculture in varying climatic conditions [5].

The first projection of nitrogen leaching into the groundwater, taking into account climate change, was prepared for individual regions of Slovenia within the framework of the *Climate change and impacts on water supply "CC-WaterS"* [6] project. Given the great uncertainty of the results of climate models (ALADIN, RegCM3, PROMIS), the simulation of nitrogen leaching with the dynamic and process-based model NDICEA (unchanged land use and agricultural technologies) [7] indicated only a slight impact of climate change on the period 2021–2050 on the extent of nitrogen leaching.

In the framework of the reporting by the Republic of Slovenia under Article 10 of the Council Directive 91/676/EEC concerning the protection of water against pollution caused by nitrate from agricultural sources for the period of 2012–2015 [8], the model-based system GROWA – DENUZ / WEKU [9] was used to model the nitrate flux through the root zone of the soil. The importance of speed and quantity of seepage water or water balance was highlighted. Time variability of annual averages of nitrate content in seepage water, which was estimated at up to 20 mg NO_3/l by individual groundwater bodies during the period 2007–2014, was otherwise associated to hydrological conditions. The effects of climate parameters on the denitrification in soil and on the rate of nitrate leaching have, however, not yet been assessed.

One of the most comprehensive overviews of denitrification simulation tools describes over fifty numerical modelling approaches [10]. The selection of the proper approach that will used in a study depends on scientific and management perspectives [11]. The most frequently used approach in Europe is a regional assessment of the impact of management practices that provides support to the implementation of the European Directives. However, the models are frequently not able to accurately represent the spatial variability of the denitrification process [12]. One of the most recent studies of the climate impact on denitrification for four districts in the Upper Danube catchment for the years 1996–2005 and 2011–2060 uses regional DANUBIA simulation system approach and shows that climate changes alone will not lead to serious changes in nitrate leaching [13]. One of the mainstream tools for exploring denitrification in terrestrial soils is the denitrification–decomposition (DNDC) model [14], which can be applied in regional as well as field site scales.

Data and methods

Using the site model DNDC [14], simulations of biogeochemical processes in the root zone of the soil were conducted for two farming scenarios [15] carried out on three representative pedological profiles [16] of the shallow aquifer layers of lower Savinja Valley. Seventy years (1946–2016) of daily climate data was used to assess the impact of climate change on the denitrification in soil and the annual rate of nitrogen leaching.

Study area

Lower Savinja Valley is an 80 km^2 large alluvial aquifer (Figure 1), represented by gravel-sandy medium to poorly permeable Pleistocene and well-permeable Holocene aquifer. There are three main terraces along the Savinja river – the lower terrace is covered with shallow eutric flu-

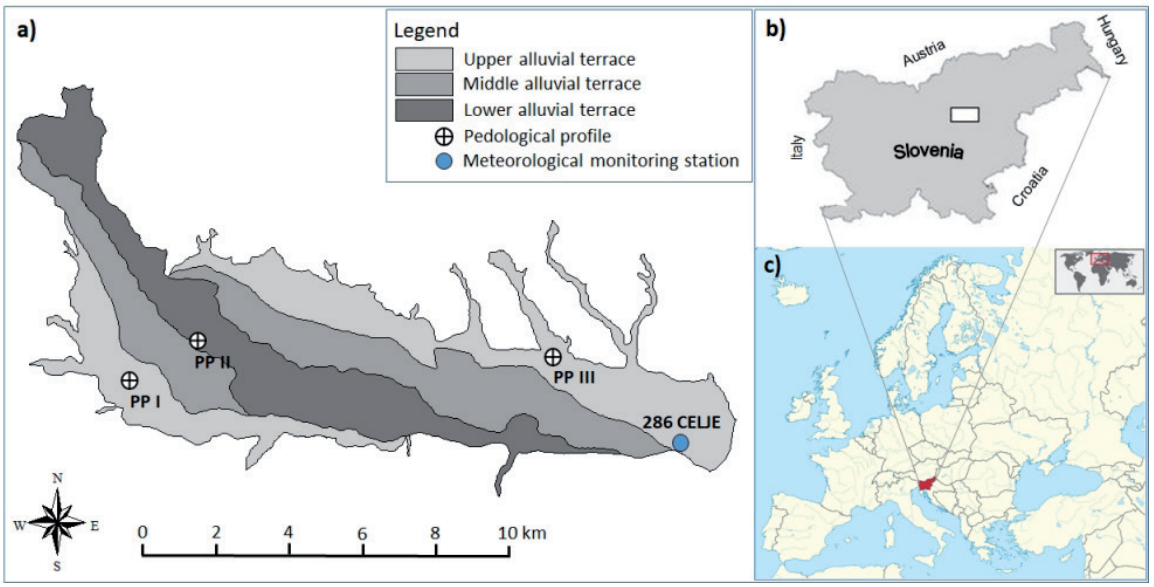

Figure 1: *Study area of Lower Savinja Valley (a), position of the study area on the map of Slovenia (b) and position of Slovenia on the map of Europe (c).*

visoil; the middle terrace on both banks of the river is covered with eutric cambisoil; and the upper terrace is covered with poorly permeable eutric gleysoil (Figure 1). Approximately half of the study area is in agricultural use, dominated by meadows, pastures, fields, gardens, as well as hopfields. The national monitoring of groundwater quality in the water management plan 2016–2021 defined the groundwater chemical status of this water body as poor, due to exceeding nitrate threshold value [1]. This water body also includes regionally important water-supply resources.

Climate data

The area of Lower Savinja Valley has the characteristics of moderate continental climate of central Slovenia [17] with peak rainfall in the summer and a great difference between winter and summer air temperatures. The Meteorological Station 268 CELJE in Medlog (Figure 1) measured the annual precipitation in the period from 1947 to 2016, ranging from 669 to 1407 mm, with the average of 1042 mm [18]. The spread between the driest and the wettest year is as much as 738 mm, and the standard deviation is 142,7 mm. This exceeds the monthly rainfall in the average vegetation period in this area. Additional to the high variability in rainfall, we also discovered great variability in air temperature, which determines the duration of the vegetation period and significantly increases the level of denitrification in the soil. In the analyzed period of seventy years, the average of the maximum daily temperatures was 15,6°C, and the average of the minimum daily temperatures was 4,3°C. The duration of the period with an average daily temperature above 5,0°C, which is the threshold of determining vegetation period, has changed greatly over the years. According to these temperature data, the start of the vegetation period ranged from mid-March to mid-April, while the end of the vegetation period ranged from mid-October to mid-November.

Pedological profiles

There are three generalized groups of soil in the study area: eutric fluvisoil, cambisoil and gleysoil. Three representative soil profiles were selected for modeling of nitrogen leaching from the soil: the Trnava profile (PP I), Orla vas profile (PP II), and Arja vas profile (PP III) (Figure 1). Input model data on pedological characteristics were drawn from the database of the pedological map of Slovenia [19], as well as from the national database of research on soil contamination in Slovenia [20]. To assess the hydraulic properties of the soil, we relied on the SAXTON [21] and the SWAP model [22],

with the latter already being tested in Slovenia on the soil of the grass lysimeter site of the Biotechnical Faculty in Ljubljana [23].

Farming scenarios

As the modeling of nitrogen leaching from the soil should primarily assess the impact of climate change on the denitrification process, we selected two simplified annual recurrent scenarios of farming practice. The first scenario (FS I) was an example of the prevailing extensive agricultural land use. The second scenario (FS II) was an example of the most intensive agricultural land use with the foreseen use of mineral fertilizers in the annual amount of 180 kg N per hectare. Model-needed data on plants were taken from the DNDC model data library [21].

Model approach

The DNDC model [14] was used to assess the impact of climate change on the level of nitrogen leaching from the root zone of soil profile, which simulates the processes between the main nitrogen pools, including denitrification (Figure 2).

The DNDC model represents the link between the environmental driving forces and the outputs from the nitrogen cycle of the soil in the form of biomass, gases and leaching. Model processes are driven by primary ecological driving forces: climate, soil and vegetation, and farming practices. The DNDC model consists of two components that solve the equations of the soil climate by calculating the water outflow and the equations of biogeochemistry of nitrogen in the soil. The first model component consists of three sub-modules: soil climate, vegetation growth and decomposition. Based on climate, soil, vegetation and farming activities data, this component enables assessment of the following soil factors: soil temperature and moisture, pH and oxidation-reduction potential, and content of substrates. The second component consists of nitrification, denitrification and fermentation submodels, enabling the simulation of the emission of gases from the soil-plant system. The DNDC model incorporates the classical laws of physics, chemistry and biology as well as empirical equations from field and laboratory studies, thus representing

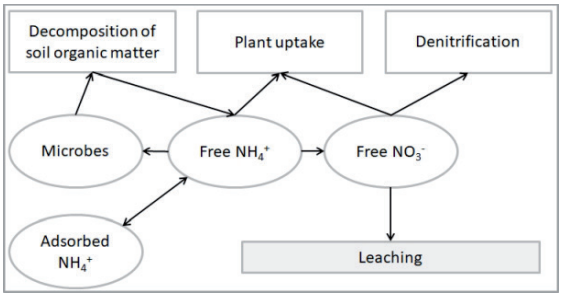

Figure 2: *Major nitrogen pools and fluxes simulated in DNDC [24].*

the connection between the carbon and the nitrogen biogeochemical cycles and primary driving forces. The simulation results of the DNDC model, applied to the study area of the Lower Savinja Valley, were evaluated by comparison to the results of the measurements of the field experiment in 2000 and the parallel simulation of nitrogen leaching in the GLEAMS model [25, 26]. The trend analysis [27] and analysis of variance [28] were performed on the timeline of the model simulations results.

The estimation of trends in time series of annual values is based on the nonparametric approaches. The presence of a monotonic increasing or decreasing trend is tested with Mann-Kendall test and the slope of a linear trend is estimated with Sen's method. These methods offer many advantages that have made them useful in analyzing climate and related data [27].

Results and discussion

The average daily air temperatures at the national meteorological monitoring station 268 CELJE in Medlog in the period 1947–2016 indicate a significant upward trend of about + 1,8 °C. A significant upward trend is also calculated for average annual minimum and maximum air temperatures. The average annual minimum air temperatures are among the most important restrictive environmental conditions for the denitrification process, and they have increased at this monitoring station with a statistically significant trend (α = 0,01) from 3,0 to 5,5 °C (Figure 3a) during the same time period. Statistically significant decrease in precipitation during the vegetation season is typical mostly for the northwestern part and

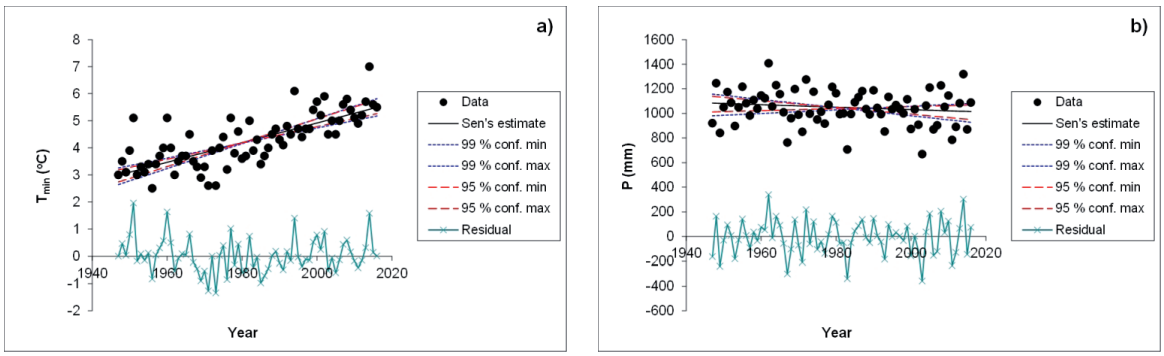

Figure 3: *Trend of average annual minimum air temperature (a) and annual precipitation (b) at the meteorological monitoring station 268 CELJE in Medlog in the period 1947–2016.*

Table 1: *Statistics of DNDC model results of the annual nitrogen leaching simulation in kilograms per hectare in the period 1947–2016.*

Pedological profile (PP)	**PP I (Trnava)**		**PP II (Orova vas)**		**PP III (Arja vas)**	
Farming scenario (FS)	**FS I**	**FS II**	**FS I**	**FS II**	**FS I**	**FS II**
Xmin	0,7	8,9	1,2	6,9	0,6	3,6
X max	6,4	39	8,8	34,7	4	14,2
Mean	2,4	24	4,2	21,3	2,1	9,6
Standard deviation	1,3	6,4	1,7	5,9	0,8	2,4
Trend Z-test	$\alpha > 0,1$	$\alpha = 0,1$	$\alpha > 0,1$	$\alpha = 0,1$	$\alpha > 0,1$	$\alpha > 0,1$

the southern edge of the country [4]. The meteorological monitoring station in Medlog, however, shows a negative trend line for the period 1947–2016, which is not statistically significant neither at the annual level (Figure 3b), nor for the level of the vegetation season, mainly due to the high variability. With these findings, the potential evapotranspiration statistically increased and impacted the amount of water in the soil, as expected. In some parts of southwestern and northeastern Slovenia, potential evapotranspiration increased by as much as 20% or more [4].

Seventy annual simulations were carried out on two representative pedological profiles (PP) for two farming scenarios (FS), accounting for 420 model launches. This gave us a satisfactory insight into the time variability of the impact of climate change on denitrification in the case of six scenarios of an agriculturally heavily burdened area in Slovenia.

The leaching of nitrogen in the case of the first two pedological profiles of more permeable cambisoil and fluvisoil deviates from leaching in the case of third pedological profile represented by gleysoils. On average, this is the difference between the annual quantity of 24 kg in the case of the pedological profile I and 9,6 kg N per hectare in the case of the pedological profile III (Table 1). Even greater differences, however, occur between the scenarios of extensive and intensive farming practice, as evidenced by the two-level nested analysis of variance. In addition to the variability between the scenarios of farming practice and the variability between pedologic profiles, our main interest in the hierarchical scheme lied in the third level of variability: the time variability of the annual amount of nitrogen leaching per hectare, calculated by the model simulation of DNDC. Taking into account the entire time period from 1947 to 2016 (n = 70), time variance compo-

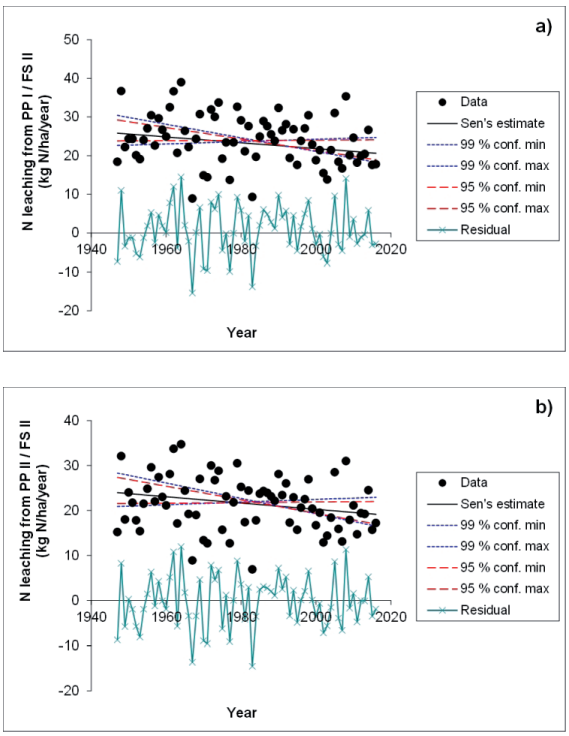

Figure 4: *Statistically significant trend (α = 0,1) of annual nitrogen leaching per hectare in the pedological profile PP I (a) and pedological profile PP II (b) while taking into account intensive farming scenario (FS II).*

nent reached 9,6%. However, this percentage drops to 8,0% of total variability of the selected three-level variance scheme when taking into account only the last water balance period from 1981 to 2010 (n = 30).

In addition to the share of the variability of nitrogen leaching, which may be contributed by the time and climate variability, the information about the annual nitrogen leaching quantity trend for individual scenarios of farming practice and for individual pedological profiles is also of strategic importance in the long-term. In all six scenarios, the trend analysis of the annual quantity of leached nitrogen reveals statistically significant downward trends (α = 0,1) only in the case of intensive farming practice (FS II) on cambisoil (PP I) and fluvisoil (PP II) (Figure 4). Based on the Sen's estimation, we can speak of reduction of the annual leaching quantity by 5,2 kg N per hectare for the first case (PP I / FS II), and by 4,8 kg N per hectare for the second case (PP II / FS II).

Conclusions

A positive trend of air temperature by 2,5°C was observed for the period 1947–2016 in the research area of central Slovenia. This is within the range of 1,1 to 6,4°C, which is the increase of global air temperature in the 21st century, predicted by the Intergovernmental Panel on Climate Change - IPCC [29]. We did not detect a statistically significant trend in the annual precipitation in the study area. This is also in line with the findings of the IPCC report, which foresees changes in the precipitation pattern in the 21st century, with more frequent and intense but short-term precipitation events.

The influence of climate variability on denitrification and nitrogen leaching from the root zone of the soil in the study area of the Lower Savinja Valley was assessed by modeling the scenarios of extensive and intensive farming practice on representative pedological profiles. Three-level nested analysis of variance revealed only 9,8 % of the variance for the entire analyzed time period. This can be attributed to climate variability. For remaining variability, the reasons need to be found in the farming practices, types of vegetation and soil properties. Statistically significant trends in the annual amount of leached nitrogen per hectare of agricultural area were found in the case of intensive farming practices in more permeable eutric cambisol and fluvisoil. A decrease in the annual quantity of leached nitrogen by 4,8 kg in the first case and 5,2 kg of nitrogen per hectare of agricultural area in the second case of model simulation was estimated with a relatively poor statistical significance for a period of 70 years (1947–2016).

The influence of the variability of climate parameters on soil denitrification and the level of nitrogen leaching in the three selected soil profiles of the study area in the central part of Slovenia is not negligible, however, the annual levels do not indicate the significance of a long-term increase in nitrogen leaching. The future studies should be extended to the regional level and should estimate the time variability of nitrogen leaching in climatically very diverse and extreme areas of the territory of Slovenia. The results of such research could provide the basis for planning of optimal farming practices in areas which are in the wider zones of aquifers

with significant quantities of groundwater for public supply of drinking water.

Acknowledgements

This article is the result of a study carried out with the help of extensive databases and under the guidance of the staff of the Slovenian Environmental Agency during my study at the Biotechnical Faculty of the University of Ljubljana and Management Center Innsbruck with the desire to deepen my knowledge of environmentally important biogeochemical processes. I would like to thank the Slovenian Environmental Agency for the access to national monitoring data, as well as relevant references and expert advice.

References

[1] MOP (2006): *Operativni program oskrbe s pitno vodo*. Ljubljana: Ministrstvo za okolje in prostor, [cited 15. 5. 2017]. Available on: <http://www.mop.gov.si/>.

[2] Uradni list RS (2016): Ustavni zakon o dopolnitvi III. poglavja Ustave Republike Slovenije (UZ70a), stran 10493, Ur. list RS št. 75/2016.

[3] Andjelov, M., Frantar, P., Mikulič, Z., Pavlič, U., Savić, V., Souvent, P., Uhan, J. (2016): Ocena količinskega stanja podzemnih voda za Načrt upravljanja voda 2015–2021 v Sloveniji. *Geologija*, 59(2), pp. 205–219.

[4] MOP (2016): *Načrt upravljanja voda*. Ljubljana: Ministrstvo za okolje in prostor, [cited 17. 6. 2017]. Available on: <http://www.mop.gov.si/>.

[5] IPCC (2014): Climate Change 2014 Synthesis Report. Summary for Policymakers, [cited 15. 5. 2017]. Available on: <https://www.ipcc.ch/>.

[6] Koeck, R. (2012): Climate Change and Impacts on Water Supply "CC-WaterS". South-East-Europe project monograph, [cited 17. 6. 2017]. Available on: <http://www.ccwaters.eu/>.

[7] Burgt, G.J.H.M. van der, Oomen, G.J.M., Habets, A.S.J., Rossing, W.A.H. (2006): The NDICEA model, a tool to improve nitrogen use efficiency in cropping systems. *Nutrient Cycling in Agroecosystems*, 74(3), pp. 275–294.

[8] Matoz, H., Nagode, P., Mihorko, P., Cvitanič, I., Dobnikar-Tehovnik, M., Remec-Rekar, Š., Rotar, B., Andjelov, M., Uhan, J., Sever, M., Zajc, M., Marolt, P., Hebat, I., Sušin, J., Verbič, J., Zagorc, B. (2016): Poročilo Slovenije na podlagi 10. člena Direktiva [!] Sveta 91/676/EEC, ki se nanaša na varstvo voda pred onesnaženjem z nitrati iz kmetijskih virov za obdobje 2012–2015. Ljubljana: Ministrstvo za okolje in prostor, [cited 17. 6. 2017]. Available on: <http://www.mop.gov.si/>.

[9] Wendland, F., Kunkel, R., Gömann, H., Kreins, P. (2007): Water fluxes and diffuse nitrate pollution at the river basin scale: Interfaces for the coupling of agroeconomical models with hydrological approaches. *Water Science and Technology*, 3, pp. 133–142.

[10] Heinen, M. (2006): Simplified denitrification models: Overview and properties. *Geoderma*, 133(3), pp. 444–463.

[11] Boyer, E.W., Alexander, R.B., Parton, W.J., Li, C., Butterbach-Bahl, K., Donner, S.D., Wayne Skaggs, R., Del Grosso, S.J. (2006): Modeling denitrification in terrestrial and aquatic ecosystems at regional scales. *Ecological Applications*, 16(6), pp. 2123–2142.

[12] Malagó, A., Bouraoui, F., Vigiak, O., Grizzetti, B., Pastori, M. (2017): Modelling water and nutrient fluxes in the Danube River Basin with SWAT. Science of the Total Environment, 603–604, pp. 196–218.

[13] Reichenau, T.G., Klar, C.W., Schneider, K. (2016): *Effects of Climate Change on Nitrate Leaching*. In: Regional Assessment of Global Change Impacts, Mauser, W., Prasch, M. (eds.). Springer: Cham; pp. 623–629.

[14] Li, C. (2009): User`s guide for the DNDC model - Vesion 9.3. University of New Hampshire, 88 p.

[15] Uhan, J. (2011): Ranljivost podzemne vode na nitratno onesnaženje v aluvialnih vodonosnikih Slovenije. Doktorska disertacija. Ljubljana; Univerza v Ljubljani 2011; 163 p.

[16] PKS, (2007): Pedološka karta Slovenije. Ministrstvo za kmetijstvo, gozdarstvo in prehrano. [cited 10. 2. 2008]. Available on: <http://rkg.gov.si/GERK/>.

[17] Ogrin, D. (1996): Podnebni tipi v Sloveniji = The climate types in Slovenia. *Geografski vestnik*, 68, pp. 39–56.

[18] ARSO (2017): Arhiv meteoroloških podatkov. Agencija Republike Slovenije za okolje.

[19] Tič, I., Vrščaj, B. (2002): Talni informacijski sistem, Slovenije – TIS : Tehnična dokumentacija. Ljubljana: Center za pedologijo in varstvo okolja, 2002; 75 p.

[20] Zupan, M., Grčman, H., Tič, I., Hodnik, A., Kralj, T., Šporar, M., Rupreht, J., Šinkovec, M., Lapajne, S., Šijanec, V., Ilc, Z., Gogič Kneževič, S., Mohorovič, B., Istenič, B., Kralj, T., Rojec, L., Rojec, M., Zupan, M., Šijanec, M. (2008): Raziskave onesnaženosti tal Slovenije v letu 2007. Ljubljana: Biotehniška fakulteta, Oddelek za agronomijo, Center za pedologijo in varstvo okolja; 105 p.

[21] Saxton, K.E., Rawls, W.J., Romberger, J.S., Papendick, R.I. (1986): Estimating generalized soil-water characteristics from texture. Soil Science Society of America Journal, 50(4), pp. 1031–1036.

[22] Saxton, K.E., Johnson, H.P., Shaw, R.H. (1974): Modeling evapotranspiration and soil moisture. Trans. ASAE, 17(4), pp. 673–677.

[23] Matičič, B., Feges, M., Saxton, K.E. (1992): Comparing measured and simulater daily water balance of a grass covered lysimeter. *ICID Bulletin*, 41(2), pp. 163–172.

[24] Pearson, T., Brown, S. (2010): Assessment of potential for development of a simplified methodology for accounting for reduction in N2O emissions from change in fertilizer usage. Report to Packard Foundation under #2008-32689, 49 p.

[25] Pintar, M., Zupanc, V., Čenčur Curk, B. (2005): *Modelling of nitrate leaching to groundwater under Slovenian conditions*. In: Nitrates in groundwater, Razowska-Javorek, L., Sadurski, A. (eds.). Selected papers from the European meeting of the International Association of Hydrogeologists, pp. 129–137.

[26] Uhan, J., Brilly, M., Pintar, M., Vižintin, G., Trček, B., Pezdič, J. (2011): *The impact of anoxic conditions on regional groundwater nitrate distribution and vulnerability assessment*. In: Groundwater: our source of security in an uncertain future: papers presented at the international conference, 19th to 21st September 2011, Pretoria, South Africa.

[27] Salmi, T., Määttä, A., Anttila, P., Ruoho-Airola, T., Amnell, T. (2002): Detecting trends of annual values of atmospheric pollutants by the Mann-Kendall test and Sen's slope estimates - The Excel template application MAKESENS. Finnish Meteorological Institute, Helsinki, 35 p.

[28] McDonald, J.H. (2017): Handbook of Biological Statistics. University of Delaware, [cited 17. 7. 2017]. Available on: <http://www.biostathandbook.com/>.

[29] IPCC (2007): IPCC Fourth Assessment Report: Climate Change 2007, [cited 21. 10. 2017]. Available on: <https://www.ipcc.ch/>.

Original scientific paper

Received: Sep 05, 2017
Accepted: Jan 03, 2018
DOI: 10.2478/rmzmag-2018-0011

Groundwater Occurrence from Hydrogeomorphological Study of Hard Rock Terrain of Part of Southwestern Nigeria

Pojavi Podzemne Vode Odkriti s Hidro-Geomorfološko Študijo Ozemlja Matičnih Kamnin v Jugozahodnem Delu Nigerije

Akanbi Olanrewaju Akinfemiwa[1,*]
[1] Department of Earth Sciences, Ajayi Crowther University Oyo, Oyo State, Nigeria
* olanrewajuakanbi@yahoo.com

Abstract

Studies of structural and hydrogeomorphological units (HGU) that are indicators of groundwater occurrence were carried out across an area extent of more than 700 km^2 within the hard rock terrain of southwestern Nigeria. These studies integrated geological remote sensing techniques (RST) and geographical information system (GIS) methods to generate thematic maps that included elevation, drainage, lineaments and vegetation index for characterising the attributes of groundwater occurrence across the area.

The results revealed that the lineament system is mainly rectilinear with major trends of NNW–SSE and NE–SW on the gneiss, NW–SE and NE–SW on porphyritic granite and NNE–SSW, NW–SE and E–W on migmatite. The discharge zones in the area are the lowland terrains underlain by gneiss and amphibolite. Similarly, variably directional discontinuities that are related to rock contacts are equally laden with groundwater.

Conversely, the recharge areas are the high-lying terrains characterised by higher fracture density and underlain by porphyritic granite and migmatite. Additionally, there are evidences of groundwater seepage along the major river channels. Therefore, besides the rock structures, landform is another crucial factor that guides groundwater distribution in the study area.

Key words: Hard rock, structures, hydrogeomorphological units, topography, groundwater occurrence

Povzetek

Pričujočo študijo strukturnih in hidro-geomorfoloških enot (HGU), ki nakazujejo pojave podzemne vode, so izvedli na več kakor 700 km^2 velikem ozemlju matičnih kamnin v jugozahodni Nigeriji. Obsegala je geološke metode, metode daljinske detekcije (RST) in GIS, kar je omogočilo izdelavo tematskih kart nadmorske višine, povodij, prelomov in vegetacijskega indeksa, ki karakterizirajo navzočnost podzemne vode na ozemlju.

Raziskava kaže, da so prelomni sistemi v glavnem premočrtni s prevladujočimi smermi NNW-SSE in NE-SW v gnajsu, NW-SE in NE-SW v porfiritnem granitu in NNE-SSW, NW-SE in E-W v migmatitu. Pasovi iztekanja na proučevanem ozemlju so v niže ležečih območjih z gnajsom in amfibolitom v globini. Podzemna voda je vezana tudi na različne linearne nezveznosti na stikih med kamninami.

Nasprotno so pa napajalne površine na vzpetinah z značilno večjo gostoto razpok in navzočnostjo porfiritnega granita in migmatita. Iztekanje podzemne vode je dodatno moč opaziti v strugah glavnih rek. Mimo kamninske zgradbe je torej tudi krajinska oblikovanost dejavnik, ki odločilno vpliva na porazdelitev podzemne vode na proučevanem ozemlju.

Ključne besede: matična kamnina, zgradba, hidro-geomorfološe enote, topografija, pojavi podzemne vode

Introduction

Crystalline basement rocks can neither store nor transmit water. Nonetheless, secondary water conduits generated from epigenetic geological events such as fractures and faults can develop within the impermeable crystalline rock units. Additionally, syngenetic structural discontinuities such as foliation and zones of rock contacts may equally be zones of water transmission in hard rock terrains, since they are zones of weakness that are more readily susceptible to weathering processes [1, 2]. These rock discontinuities are the rock structural elements that are collectively regarded as lineaments when they are mappable over an area. Lineament can easily be mapped from the outcropping rock sections. However, in areas where there are no outcrops and where the hard rocks have been weathered or buried by recent deposit and regolith, the structures are most of the time invisible and undetectable, except by applying remote sensing techniques (RST).

The principle of remote sensing revolves around the physical attributes of natural ground objects in response to their distinguishing abilities to reflect, emit and absorb different intensities of radiation at different ranges of electromagnetic wavelength. The use of satellite imageries is one way of applying RST for groundwater investigation, and it has been found to be helpful for regional groundwater exploration of terrains with large area coverage [3, 4]. Besides the geological setting of an area that has a strong bearing on groundwater prospect of the area, hydrogeomorphological units (HGU) in the form of thematic maps produced from appropriate satellite imageries are also vital in any groundwater study.

To a large extent, the application of remote sensing techniques (RST) in hydrogeomorphological studies of various landforms has been undertaken in more advanced nations [5, 6], and it is now becoming popular in developing nations of the African continent. For example, increase in the borehole success rate and reduction in the costs of groundwater exploration were linked to the application of RST for lineament interpretation in Ghana [7]. Nevertheless, there is need for more comprehensive approach in the application of RST to groundwater exploration. This is more crucial in the hard rock terrains of southwestern Nigeria where groundwater potential is poor and the borehole success rate is just about 30% [2, 8]. Hence, besides lineament studies, the present work also applies RST to study other HGU that are indicators of groundwater such as landforms, surface water network pattern and vegetation index.

Site Description and Geological Setting

The study area occupies 711.17 km^2 landmass area of the Ibarapa region within southwestern Nigeria on coordinates N7° 21′ to N7° 37′ and E3° 07′ to E3° 21′ (Figure 1). The major towns within the area are Igbo-Ora, Idere, Ayete and Tapa with a total population of 204,071 as per the last census conducted in 2006 [9]. With the human growth rate of 2.9% in Nigeria [10], it is expected that human population would have tripled in these communities. In respect of climatic conditions, the study area lies within the tropical climatic zone, which is marked by two distinct wet and dry seasons. The dry season extends from November to March with an average monthly precipitation of less than 25 mm. The wet season peaks around June and September with the monthly rainfall exceeding 100 mm. The total annual rainfall in the area ranges from 813 to 1853 mm, whereas the annual temperature ranges from 24°C to 29°C.

Like many cities, towns and rural settlements in Nigeria, Ibarapa town water supply scheme, which is largely sourced from surface water, has long been abandoned and houses are not connected with piped water facilities. Hence, for domestic water needs, and even for agricultural purposes, residents of Ibarapa areas rely on groundwater supply tapped from hundreds of hand-pump boreholes that were drilled for the communities across the area. However, even with these provisions, availability of potable water is still inadequate, largely due to the unsustainable yield of many of the functioning boreholes. This scenario is further complicated as a result of increasing human population in Nigeria that has an attending increasing demand on fresh water supply. This demand has made it mandatory to increase the present groundwater supply. However, the Ibarapa region is mainly underlain by crystalline basement rocks that ordinarily have little or no po-

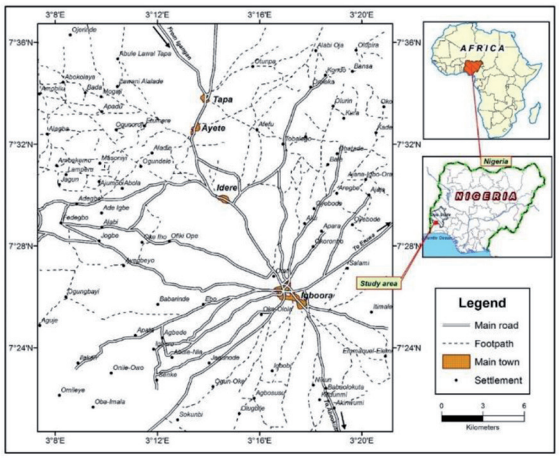

Figure 1: *Location map of the study area.*

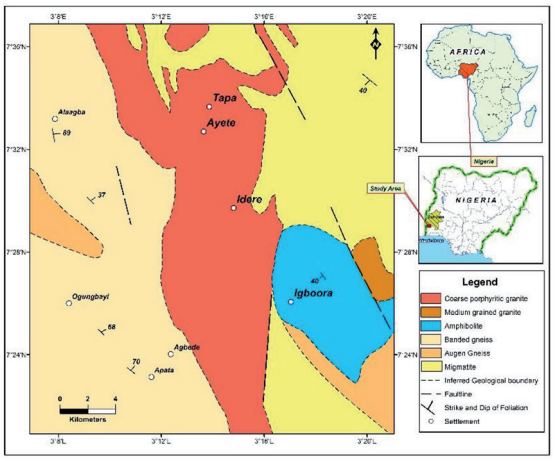

Figure 2: *Geological map of the study area (modified after Weerawarnakula, 1986).*

tential for groundwater except where there are enough rock structures that are interconnected and development of a significant regolith thickness and/or occurrences of fractured bedrocks that aid groundwater transmission [11–13]. Therefore, the use of processed satellite imageries for geomorphological and structural studies of the Ibarapa region will provide insight into groundwater potential across this region, which is underlain by diverse crystalline rocks.

The principal rock units are granite varieties that include coarse porphyritic granites and medium-grained granites, banded and augen gneissic rocks, amphibolite and migmatite. The distribution of the major rock units in the study area is shown in Figure 2. The outcrop exposures of porphyritic granite occur at the central part and occupy about one-third of the entire study. However, outcrops of the medium-grained granites are isolated and underlain comparatively much smaller area at the eastern part of the study area [2].

Amphibolite underlies most part of Igbo-Ora township and has massive and schistose varieties. The lineation trend ranges from 093° to 124°, and the foliation dips between 38°W and 44°W [13] for the schistose variety. Banded and augen gneisses are foliated metamorphic rocks. The foliation of the banded gneiss trends northerly between 339° and 360° and dips vertically eastward close to Alagba at the NW region. The foliation dips between 68°E and 70°E at the WSW region and 37°E at the WNW area. Banded gneiss underlies most part of the western part of the study area. Augen gneiss occupies small sections and is found as older rock units within the banded gneiss at the western and southeast parts of the study area. The migmatite is the oldest rock unit across the study area, and just like banded gneiss and porphyritic granite, migmatite also has an extensive area coverage. Migmatite outcrops dominate most adjoining villages such as Kondo, Obatade, Tobalogbo and Alabi Oja at the northeastern part (Figure 1).

Materials and Methods

For geological and geomorphological studies of the area, field methods are crucial but are not efficient for large area coverage. In addition, relying on field data alone provides limited information on the persistence or spatial continuities of structures that are significant for groundwater occurrence. Hence, the present study integrated field mapping, remote sensing methods and application of geographical information system (GIS) techniques for extracting and inferring both the geology and the HGU from available information, maps and satellite imageries.

Field Mapping

The geological studies involved the conventional mapping of rock units and measurement of the structural elements on outcropping sections with the aid of compass clinometer. From this exercise, the available geology map of the

area was updated and rock boundaries were accurately fixed. Location coordinates of rock types and rock structures such as fractures and faults and locally available information on other HGU including elevations and locations of surface water bodies were taken on site with the aid of Garmin eTrex GPS. These data were used as guides for interpreting information from the satellite images.

Satellite Images

Downloadable satellite imageries that were used for the present work are the shuttle radar terrain model (SRTM) bands of radar and the normalised difference vegetation index (NDVI) images from Landsat. These imageries are available globally and freely provided by National Aeronautics and Space Administration (NASA). The images were shot at the peak of dry season and were used for hydrogeological interpretation of the crystalline areas of the Ibarapa region.

Radar

The radar satellite images are readily applicable for interpretation of many significant parameters of hydrogeological importance such as terrain analysis, lineament mapping and geologic interpretation. The SRTM owned by NASA is a name given to the C and X radar bands that have a frequency range of approximately 3–10 GHz and a resolution of 25–90 m. The SRTM is the digital elevation model (DEM) of radar, which has strong application to the land surface relief and can give a 3D elevation impression of the study area. The absolute height accuracy of DEM is 16 m, and the relative accuracy is <10 m. SRTM data in the form of DEMs are available globally between 60°N and 58°S. The SRTM data have to be imported into ArcGIS for producing both the 2D and 3D terrain elevation from which the landform of the area is generated. It is also applicable for characterising the lineament and drainage network of the study area.

Landsat Thematic Mapper (TM)

Landsat TM is an advanced multispectral scanner used in Landsat 4 and 5 missions. It has seven ranges of wavelength specifications. Bands of red, green and blue (RGB) and thermal infrared (TIR) were processed and used for specific hydrogeological investigations in the present work. The RGB Landsat bands have a ground resolution of 30 m, while the TIR has a resolution of 120 m [14]. For structural characterisation of hard rock terrains, the TIR Landsat band is quite influential for delineation of structural (lineament) features such as folds, fractures, faults and foliation. Besides lineament features, the TIR band is also applicable for studying other hydrogeomorphologic features such as surface water flow and groundwater recharge [15, 16]. These HGUs are distinguishable as a result of spatial differences in thermal characters of rocks. For example, lineaments that are conduits for water will produce traceable linear features due to the contrast in heat variations along the region of groundwater flow. In addition, in Landsat ETM, the three primary colours, namely blue, green and red, are assigned to 0.45–0.52, 0.52–0.60 and 0.63–0.69 μm spectral bands, respectively. Hence, the vegetation of the area is processed from the NDVI since green vegetation reflects much light in the near infrared (NIR) band than in the red (RED) band. Hence, the difference between the two bands (i.e., NIR–RED) will give the vegetation index. The difference in reflection (known as DNs) of the NIR and RED bands is much greater for green vegetation than for bare soils, rock exposures, water bodies, etc. An image containing pixel values of the difference is termed a vegetation index image. However, due to a large range of spectral signature that can be generated from DNs, the difference is normalised by dividing it by the sum so that the range of NDVI values will lie between -1 and 1. Hence, pixels with lush vegetation on an NDVI image that are often assigned to high values appear as whitish tones, while those with no or poor vegetation appear as dark grey to black tones.

The NDVI is applicable for detecting water-bearing lineaments. This application of NDVI assumes that vegetation respond to presence of water; hence, areas with plant lushness are characterised by water-containing fractures. This explanation is also used to detect groundwater recharge zones across the area. Nonetheless, for the present study, the NDVI is presented in colour composites for better image enhancement. The colour composite

image of NDVI has an edge over the ordinary one, since interpretation in the latter considers light and dark tones for distinguishing features. However, in the colour composite image, the high-tone spots in NDVI are now seen as green colour spots, which represent locations with lush vegetation.

Processing of Data

The processing involved the applications of GIS techniques using Erdas Imagine and ArcGIS software for extracting data and for generating visual and digital thematic maps from the satellite images. In addition, the GIS is used for superimposition of the structural lineament map on the geological map to characterise the lineament units across the various bedrock terrains. The processed thematic maps produced for the entire site of investigation included the surface drainage network, structural lineament, DEM and NDVI. The first three maps, in addition to the geology map, were used to characterise the groundwater potential of the terrain, while the NDVI indicated the actual groundwater occurrence across the area. The peculiarity of the NDVI is that it reflects groundwater occurrence from vegetation response of the area if the area is irrigated naturally by underground waters. This is considered appropriate for the present study, since the area met the conditions for applying the NDVI as groundwater occurrence indicator. The area was not artificially irrigated, and the satellite imageries used were taken in the month of February at the peak of dry season in the Ibarapa region. This translates that the source of irrigation water is subsurface and not meteoric. The lushness and the orientations of vegetation on the ground indicate availability of groundwater along the direction of fracture orientation. It can also be extrapolated that the presence of riparian forest along surface water drainage such as river or stream is an indication of water seepage into the subsurface environment along that channel. Hence, the NDVI was also used to identify recharge zones across the study area.

In respect of lineament characterisation, it is known that all rock discontinuities such as fractures, faults and even rock contacts act as storage and conduits for water [17, 2], and are important hydrogeological units in basement complex terrains [19]. Hence, the attributes of lineaments including the linear density (or frequency), continuity (persistence) and direction of alignment were differentiated spatially. The persistence or continuity of lineament influences the degree of structural interconnectivity, which aids water transmission in any hard rock terrain. Conversely, the DEMs produced from SRTM were used in mapping the variations in terrain elevations across the study area. In addition, they were applicable for ascertaining the topographic features (landforms) associated with individual rock-type terrain in the area [18–20]. In addition, from the DEM, the surface water drainage and structural lineament were also traceable by incorporating the enhanced image into ArcGIS and Edras Imagine GIS software.

Results and Discussion

Landforms

The 2D and 3D DEMs of the study area are correspondingly shown in Figures 3a and 3b. The geomorphology of the area is characterised by wide landforms contrast that included hills or inselbergs, highlands, lowlands and floodplains (Figures 3a and 3b). The hills and ridges are found at the central upper section of the area, spreading across most of the major towns, namely, Tapa, Ayete and Idere. Inselbergs are also associated with the northwest and northeast regions. These highly elevated landforms are separated by incision of valleys and lowlands that are drainage channels in the high-lying terrains. Most of these hills and ridges are porphyritic outcrops with elevations exceeding 300 m above the sea level. Terrain elevation drops from Idere toward the northeastern part to high ground or highlands that are mainly underlain by migmatite. There is also a small section of highlands at the western part of the gneissic bedrock terrain. The elevations of highlands are within 250–300 m. Terrains with elevations that range between 250 and 150 m are the lowlands. The underlying rock units that constitute the lowlands are gneisses and amphibolite. Lowland landforms are flat-lying plains and spread across the western and the southeastern parts of the area. Lastly,

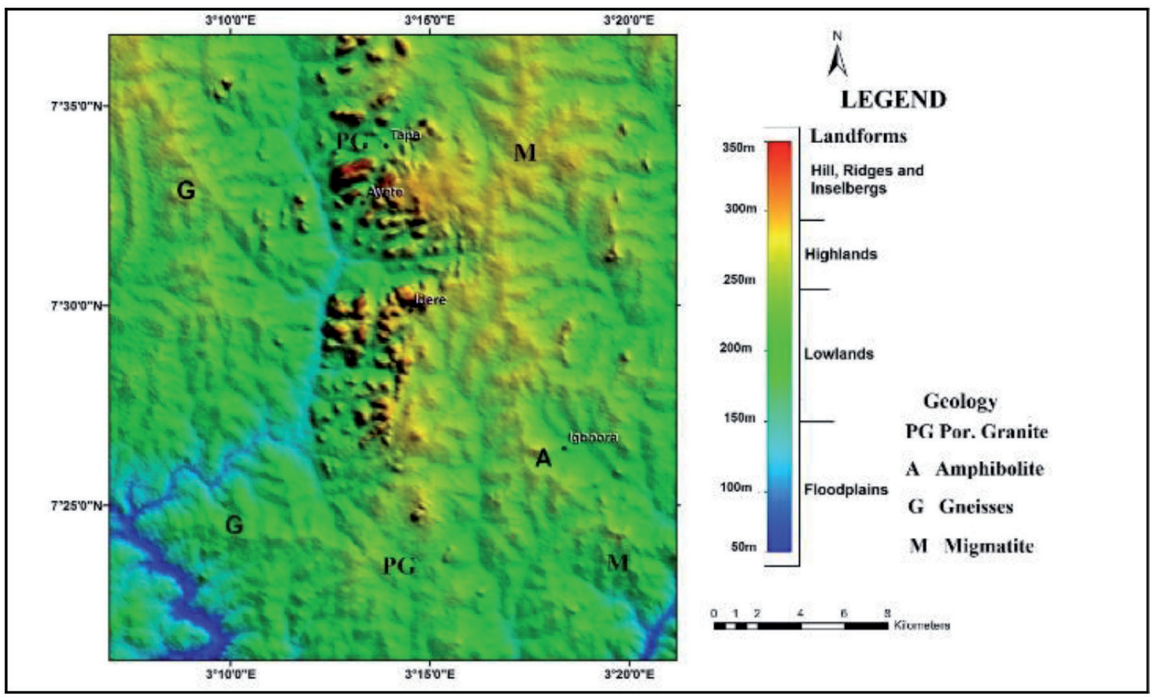

Figure *3a: 2D DEM of the study area.*

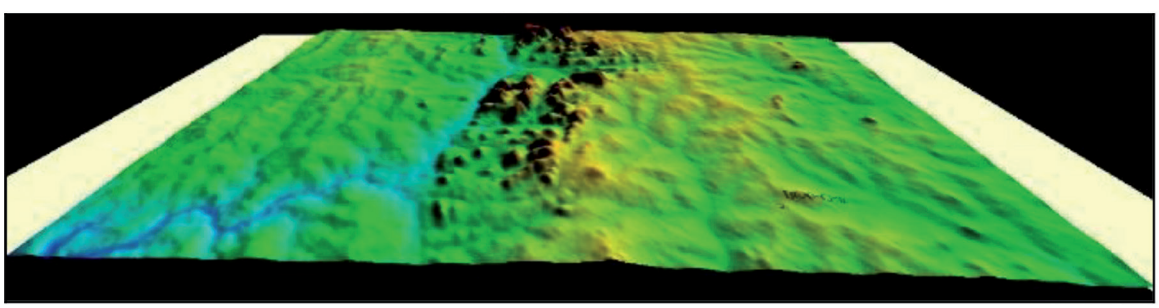

Figure *3b: 3D DEM of the study area.*

the floodplains are land depression terrains with elevation less than 150 m. Floodplains are prone to flooding and sediment deposition from transported regolith of the upland areas. In terms of area coverage, the floodplains occupy the smallest area and are restricted to small sections in the southwest and southeast parts of the area, the former floodplain being larger than that on the migmatitic terrain at the southeast (Figure 3a).

Usually, the high topographic terrains are regarded as recharge areas characterised by deeper water table and high hydraulic gradient. Low-lying areas are normally the discharge zones where the water table is shallow and close to the surface environment [1]. Hence, based on the topographic consideration alone, areas underlain by porphyritic granite and migmatite are the recharge points, while amphibolitic and gneissic terrains are expected to have better groundwater potential with respect to groundwater yield and sustainability.

Drainage and Watershed

The drainage pattern is dendritic (Figure 4) as typical of basement areas marked by high contrast in relief. The surface drainage network consists of rivers, namely, Iworo, Ayin, Afo-Ape, Opeki, Aboluku and Ofiki. However, River Ofiki is the most prominent river that traverses and drains large part of the northern area including the granitic terrain at the central region, part of

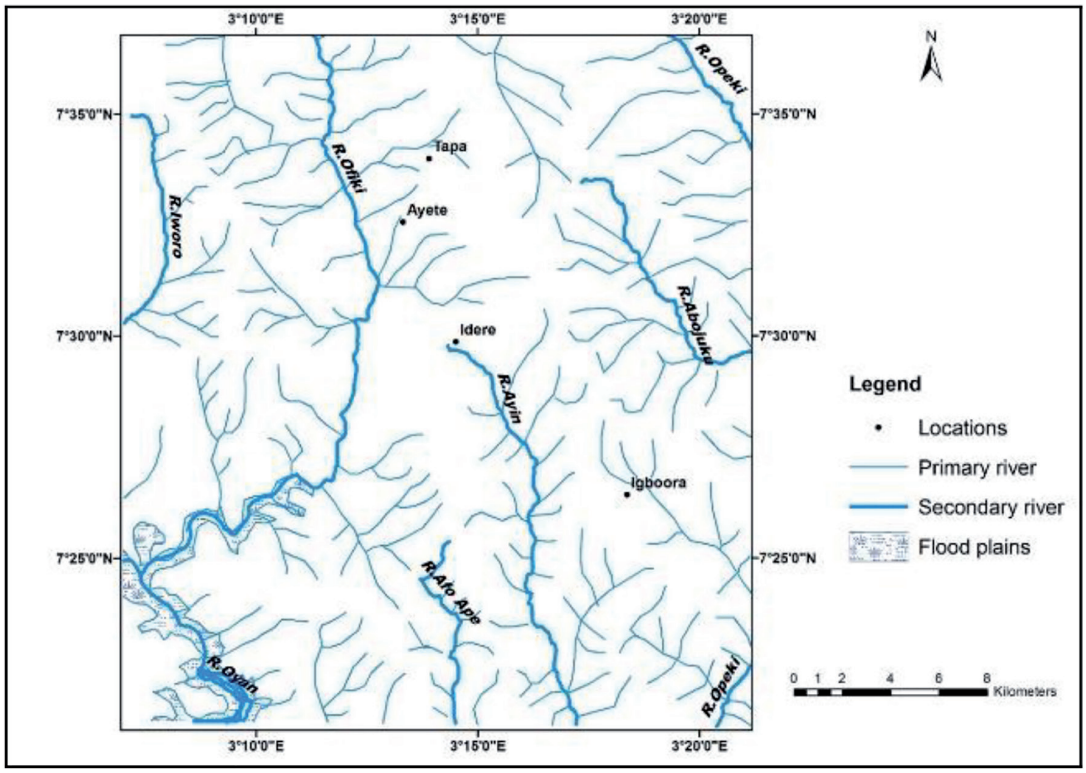

Figure 4: *Drainage pattern of the study area.*

area underlain by banded gneiss at the WNW region and up to the migmatitic terrain boundary north of Idere. The drainage pattern breaks the entire study area into different interfluves whereby each interfluve is an eroded inland area drained by a river network. By connecting interfluves that drains into the same secondary river, the entire area was partitioned into five watershed units that were named after the secondary river draining the area. These include Iworo at the NW, Ofiki at the central west, Afo-Ape at the south central, Ayin at the south central east and lastly the Aboluku-Opeki watershed extending from the east to the northeast.

The Iworo watershed is underlain by banded biotite gneiss steeply dipping west. River Iworo flows along the N–S direction, along the strike of the rock foliation. River Ofiki, which is the longest and the most prominent river, merges into River Oyan at the southwestern part of the study area. The tributaries of River Ofiki drain most part of inland regions of Oye-Igangan, Tapa, Ayete and Idere towns. This watershed has the most contrasting relief, ranging from the centrally high topographic landforms of porphyritic granite and porphyroblastic gneiss that peak at 350 m above the sea level. The Afo-Ape watershed is a minor watershed located at the central southern part of the study area that is underlain by porphyritic granite. It is a lowland with elevation below 150 m above the sea level. However, the central portion is dominated by inselbergs as well as relief up to 300 m above the sea level. The Ayin watershed covers the main township of Igbo-Ora and Idere with their adjoining areas. This region is the most complex in terms of rock types. The northern section of the Ayin watershed is underlain by granite with the associated high-rising landforms. This area encompasses Idere town and its environs. At the west, the underlying rock type is migmatite; the southwestern region is underlain by amphibolite and lastly, the Aboluku–Opeki watershed is mainly underlain by migmatite.

Structural Lineaments

The structural lineament thematic map is presented in Figure 5. This map revealed that lineaments are mainly of rectilinear type, which

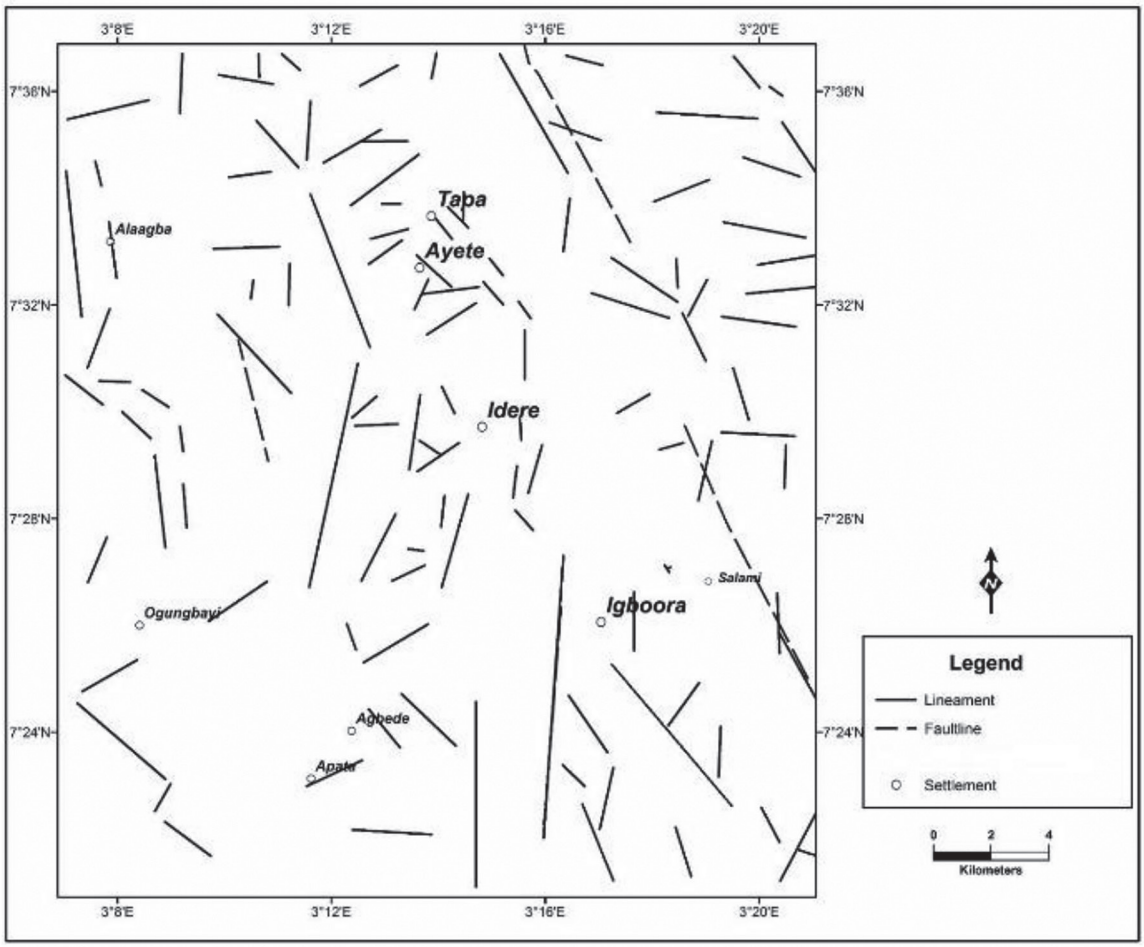

Figure 5: *Structural map of the study area.*

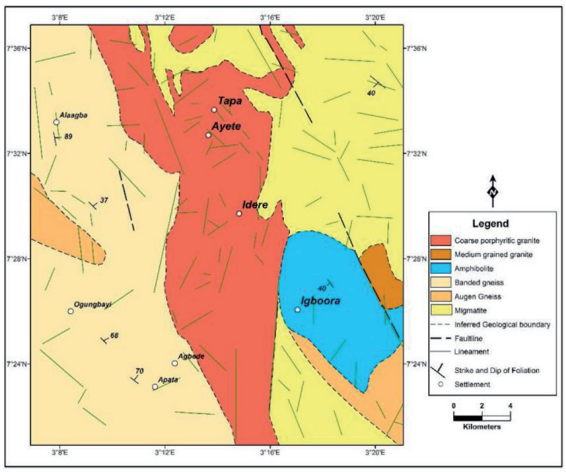

Figure 6: *Updated geological map of the study area with structural lineaments.*

indicates the brittle nature of the hard rocks that underlain the area. However, evidence of ductile behaviour represented by curvilinear fractures existed at the south of Alagba at the western part of the study area, which is underlain by biotite gneiss where foliation planes dip almost vertically (Figure 6). Obviously, there are spatial disparities in lineament attributes across the study area (Figure 5). The variation in structural units across the various hard rock terrains is shown by the superimposition of lineaments on the geology map in Figure 6.

The degree of rock brittleness is more intense at the central region underlain by porphyritic granite, which is characterised by high topographic landforms (Figures 3 and 6). These granitic terrains are associated with more numerous but short-length lineaments of linear density 0.25 km^{-1} compared to other parts of the study area (Figure 5). Notwithstanding, lineaments within the migmatitic and gneissic terrains, correspondingly at the northeast

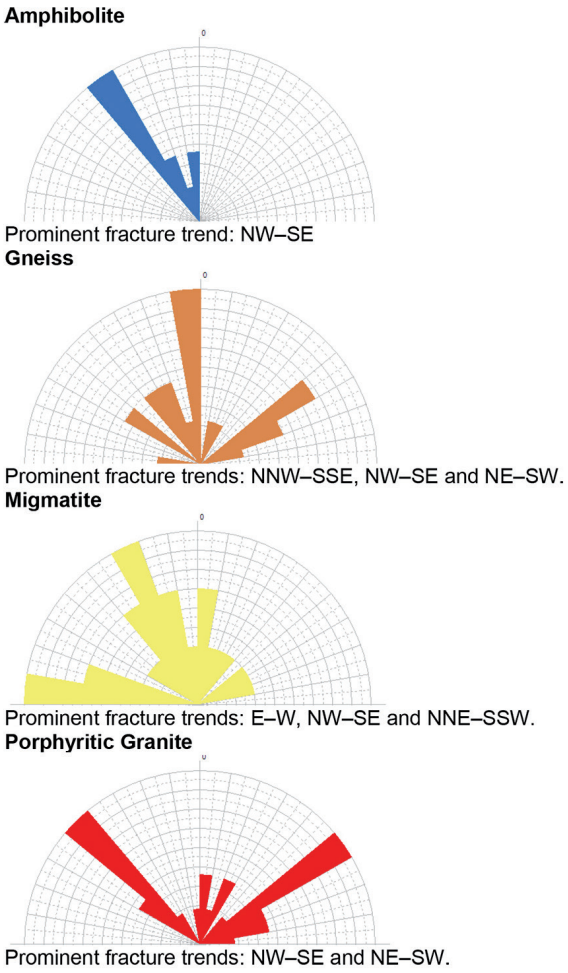

Figure 7: *Rose diagrams of lineaments/fractures obtained for the various bedrocks, illustrating the prominent orientations.*

and northwest areas, were dominated by more extensive and persistent structural units but at lower densities of 0.18 and 0.17 km^{-1}, respectively. Similarly, at the southern part of the area, porphyritic granitic terrains at the south-central portion are also characterised by higher lineament concentration with a density of 0.14 km^{-1} compared to that of 0.06 and 0.10 km^{-1} obtained for southwest and southeast portions underlain by gneiss and amphibolite, respectively.

Furthermore, Figure 6 revealed that most of the mega fractures occurred at rock contacts. In fact, River Ofiki, which is the major river that drains the study area, traverses the boundary between porphyritic granite and gneiss at the western part (Figures 3–6). In addition, at the east, occurrences of mega-linear features were associated with rock contacts between porphyritic granite and migmatite at the north and in-between porphyritic granite, migmatite and amphibolite at the south-east area. Porphyritic granitic terrains that are associated with a high fracture frequency are characterised by disjointed and less persistent (or mega) lineaments compared to gneissic and migmatitic terrains. However, at porphyritic granite boundaries with other rocks, the lineament persistence is large (Figure 6).

The orientations of linear features as shown in rose diagrams in Figure 7 are multidimensional except on amphibolite where the major fracture's trend is along the NW. In gneisses, the prominent fractures' trends are NNW–SSE, NW–SE and NE–SW. Likewise, migmatite bedrocks are characterised by three dominant linear trends, which are E–W, NW–SE and NNE–SSW, and porphyritic granite bedrocks by two major trends, which are NW–SE and NE–SW.

Vegetation Index

The NDVI colour composite of the area is presented in Figure 8. Pockets of localised groundwater zones represented by lush vegetation occur in some parts of the area. In addition, zones of recharge or water seepage signified by riparian forests are found to be associated along some river channels. However, the attributes of these groundwater occurrences are diverse and are symbolised by rings and arrows as shown in Figure 8. The white rings represent localised areas of groundwater occurrences. The white arrows show groundwater zones that are prominently controlled by the mega structural lineament in that area, while the red arrows indicate surface water channels along which water seepage or groundwater recharge occurs.

The clustered nature of lush vegetation demarcated by white rings revealed that groundwater is found in diverse lineament trends in these areas (Figure 8). On the other hand, there are evidences of occurrences of groundwater in major lineaments at some locations. This is prominent around the Alagba area at the northwest region, where lush vegetation is linearly oriented along the major structural trend in that area (Figure 8). This conspicuous groundwater occurrences trend NW–SE (Figure 8), and this trend is the strike of the mega fracture in that location

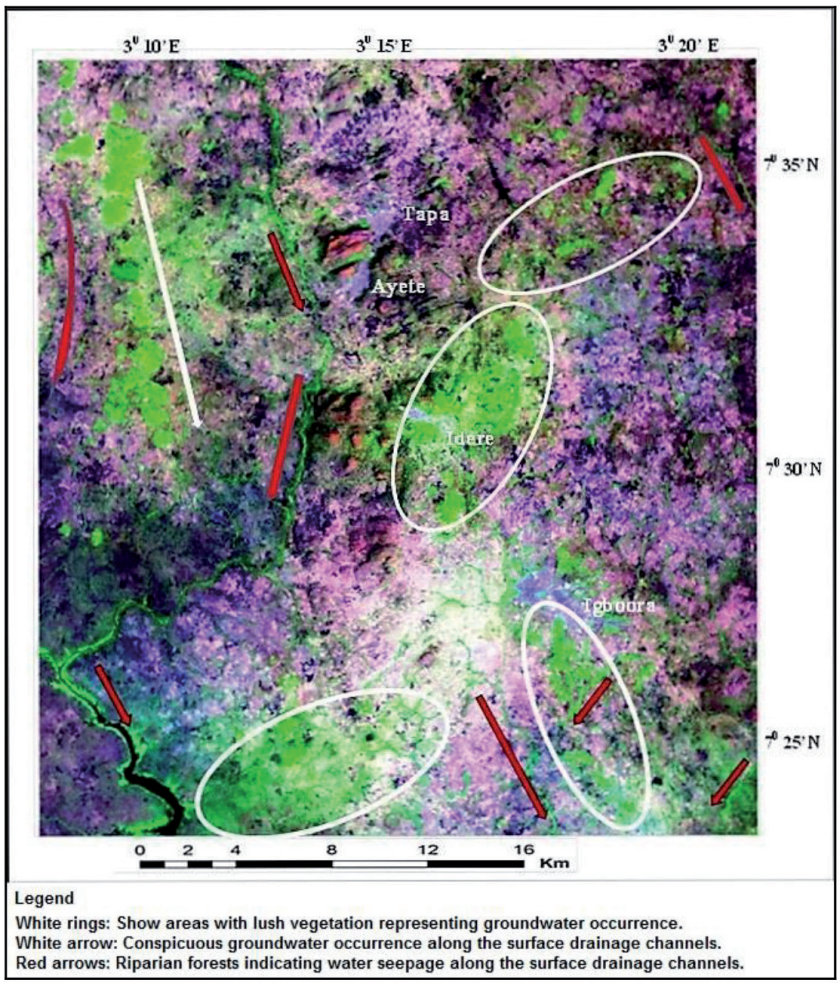

Figure 8: *Groundwater indication from colour composite NDVI image.*

(Figure 6). In this region, the underlying hard rock is banded gneiss, the foliation plane dips vertically and the direction of mineral alignment is NW–SE (Figure 2). The direction of alignment of the groundwater occurrence is the same direction at which the mineral constituents are aligned in this area (Figure 8). This revealed that the directions of mineral alignment in foliated rocks are likely zones of structural weakness for fracture generation and potential zones of groundwater occurrence in the hard rock terrain. The topography of the area is low–moderate-lying terrains, comprising valleys and moderate highland ridges that are oriented along the strike of rock foliation (Figures 2 and 3). The prominent groundwater occurrence in the area is oriented along the NW–SE strike ridge in-between rivers Iworo and Ofiki (Figures 4 and 8). This groundwater zone is recharged by River Ofiki due to evidence of water seepage along its channel (Figure 8).

Conversely, riparian forests, which are indicators of water seepage along the surface drainage network, are found across the area (Figure 8), although it is mostly prominent along River Ofiki, which drains substantial area of the northern section and traverses rock boundaries between banded gneiss and porphyritic granite to migmatite boundary at the north of Idere (Figures 4, 6 and 8). Likewise from Figure 8, it is obvious that rock boundaries are also viable groundwater zones in the area due to lush vegetation associated with zones of rock contacts. This is particularly noticeable at the centre portion around Idere and other locations at the southern parts (Figure 8).

Apart from terrains around rock contact zones, groundwater occurrences are found to be con-

fined to terrains underlain by amphibolite and gneiss (Figures 2 and 8). The topographic features in amphibolitic and gneissic terrains are low-to-medium-lying terrains (Figure 3). Conversely, groundwater occurrence is at the lowest at the north–north and most parts of the northeastern region of the study area (Figure 8), which is associated with high topographic landforms (Figure 3). These high-lying terrains are underlain by porphyritic granite and migmatite (Figure 2), and the terrains are characterised by generation of thin riparian forests and sparse vegetation response (Figure 8). Hence, locations of low-lying areas underlain by amphibolite and gneiss are the discharge zones, while the high-lying areas of porphyritic granitic and migmatitic terrains are the recharge zones within the study area. This is buttressed by the fact that the fracture density is high on granitic and migmatitic terrains (Figure 6). Although the persistence of fractures is low on the former terrain, there are extensive and more persistent lineaments associated with migmatitic terrains (Figure 6). Furthermore, despite the extensive and high fracture frequency associated with terrains underlain by porphyritic granite and migmatite (Figure 6), groundwater occurrence is still poor (Figure 8). This is typified by sparse vegetation cover and infrequency of riparian forest at the north–north and northeastern regions (Figures 2 and 8). This confirms that the infiltrated water through the numerous fractures is summarily transmitted into the adjacent low-lying terrains underlain by amphibolite and gneiss. In addition, the fact that these regions are associated with sparse vegetation suggests that the water level is far from the land surface. Notwithstanding, there are few small-sized water-laden fracture distributions scattered across the migmatitic terrain at the northeastern part (Figure 8). More so, it is also expected that the rates of overland and interflow will be high in high topographic areas underlain by porphyritic granite and migmatite, so that meteoric water is transmitted into adjacent low-lying areas underlain by amphibolite and gneiss (Figures 2 and 3).

Table 1 gives the concise details of the facts extracted from the thematic maps and the interpreted groundwater occurrence under each watershed units with their respective underlying bedrocks. For example, the Iworo watershed that is underlain by banded gneiss at the NW region is characterised by strike ridges with adjacent valley landforms (Figure 3a). The lineaments strike the NNW–SSE direction, and the foliation dips vertically (Figure 2). Groundwater occurrence is conspicuous along the strike of the foliation in this region. The Ofiki watershed traverses large area with lot of diverse topographic features ranging from lowlands at the WNW region to granitic highlands at the north-central region that extends through Tapa, Ayete and toward the migmatitic terrain boundary north of Idere. Groundwater occurrences are indicated by evidences of groundwater recharge from generation of riparian forests along the main channel of river Ofiki (Figure 8). However, groundwater zones are in variable directions and less linearly oriented at rock contact zones around Idere at the north-central section. The Ayin and Afo-Ape watersheds are mainly granitic terrains but also extend to part of rock contact zones in-between migmatite, augen gneiss and amphibolite (Figures 2 and 4). Groundwater occurrence is fair at rock contact zones with minor recharge along river Ayin (Figure 8). Lastly, Opeki and Aboluku watersheds are mainly underlain by migmatite at the NE and amphibolite at the SE. Groundwater occurrence is localised in small compartments. Rock contact zones also show fair prospect for groundwater.

Conclusion

The occurrence of groundwater in the study area is guided by topographic and structural influences. The clustered groundwater occurrence at rock contact zones showed that the orientations of the water-laden fractures are multidirectional. However, there are possibilities of locating major groundwater zones along mega lineaments whose structural outline is defined by the alignment of local rock foliation. This method of research is readily applicable for demarcating zones of groundwater potential for further groundwater development in hard rock terrains characterised by diverse geological and geomorphological settings.

Table 1: *Attributes of groundwater occurrence interpreted from HGU.*

S/n	Watershed units, region	Underlying rock type	Landform	Lineament characterisation	Vegetation response	Interpretation of groundwater occurrence
1	Iworo, northwestern section	Banded and augen gneisses	Moderate highland, strike ridges with adjacent parallel valleys	NNW–SSE trending fractures, some of which are curvilinear, indicating mega-fold structure	Linearly oriented lush vegetation along the NNW–SSE trendingfracture	Abundant groundwater occurrence. Groundwater discharge is directional and found in the NNW–SSE fractures that trend along the strike of the local foliation in the area
2	Ofiki-Oyan, southwestern section	Banded gneiss	Lowlands and floodplains	Less dense but persistent along which the river flow	Riparian forests along the river channel and clustered vegetation at rock contact zones at the south	Groundwater recharge along the river channels. Groundwater occurrence at variable directions in the rock contact zone at the south
	Ofiki, middle-belt northern section	Porphyritic granite	Hills and inselbergs with adjacent valley incisions	Fracture frequency is high but persistence is low, typifying high degree of rock brittleness. Fractures with variable orientations along the NEE–SWW, NNE–SSW and NE–SW directions	Sparse vegetation along the river bank. Lush-clustered vegetation at the rock contact zone at the middle section around Idere	High fracture density but poor groundwater occurrence. Recharge zone with deep water table, beyond the reach of plants. Groundwater occurrence in variable directions within the contact zones at Idere
3	Ayin-Afo Ape, middle-belt southern section	Porphyritic granite and rock contacts	Granitic ridges at the upper middle section. Lowlands at the lower middle section	Fairly numerous and more persistent fractures compared to the upper granitic terrain	Presence of sparse riparian forests along the channels but the weight. Fairly clustered vegetation at the rock boundary zones in the south	Low water seepage along river channels and tributaries. Fair groundwater occurrence at rock contact zones
4	Opeki and Aboluku, northeastern section	Predominantly underlain by migmatite	Highlands with inselbergs	Numerous and extensively persistent fractures aligned toward E–W and NW–SE trends	Scarce, a few small-to-medium-sized pockets of scattered vegetation. Riparian forest is scarce	Groundwater recharge area. Depth to water table is deep
	Opeki and Aboluku, southeastern section	Migmatite, amphibolite and rock contact zones	Low-to-medium-lying landform	Fractures fairly dense and more persistent along rock contacts	Clustered at rock contacts and riparian forests are fairly present	Groundwater discharge zones at rock contact and on amphibolite with variable orientation

References

[1] Fetter, C.W. (2007): *Applied hydrogeology*. 2nd edition. USA: Merrill Publishing Company.

[2] Akanbi, O.A. (2017): *Hydrogeological Characterisation of Crystalline Basement Aquifers of part of Ibarapa Area, Southwestern Nigeria.* Ph. D. Thesis. Ibadan-Nigeria: University of Ibadan 2017; 312 p.

[3] Pierce, L.L., Walker, J., Dowling, T.L., McVicar, T.R, Hatton, T.J., Running, S.W., Coughlan, J.C. (1993): Ecohydrological Changes in the Murray-Darling Basin. III. A Simulation of Regional Hydrological Changes. *Journal of Applied Ecology*, 30(2), pp. 283–94.

[4] Tweed, S.O., Leblanc, M., Webb, J.A. and Lubczynski, M.W. (2007): Remote sensing and GIS for mapping groundwater recharge and discharge areas in salinity prone catchments, southeastern Australia. *Hydrogeology Journal*, 15(1), pp. 75–96.

[5] Philip G., Singhal, B.B.G. (1992): Importance of geomorphology for hydrogeological study in hard rocks terrain, an example from Bilhar Plateau through remote sensing. *Indian Journal of Earth Sciences*, 19(4), pp. 177–188.

[6] Sreedevi, P.D., Subrahmanyam, K., Ahmed, S. (2005): Integrated approach for delineating potential zones to explore for groundwater in the Paguru River Basin, Cuddapah District, A.P., India*. Hydrogeology Journal,* 13(3), pp. 534–543.

[7] Sander, P. (2007). Lineaments in groundwater exploration: a review of applications and limitations. *Hydrogeology Journal*, 15(1), pp. 71–74.

[8] Wright, E.P. (1992): *The hydrogeology of crystalline basement aquifers in Africa*. In: Hydrogeology of crystalline basement aquifers in Africa, Wright, E.P., Burgess, W.G. (eds.) Geological society special publication No. 66. Geological society: London.

[9] *Nigeria's 2006 Population Census Arranged by State [*online], Available on: <*http://www.nigerianmuse.com/./nigeria-2006-population-census-arranged-by-state-wikipe>*

[10] Tartiyus, E.H., Mohammed, I.D., Amade, P. (2015): Impact of Population Growth on Economic Growth in Nigeria (1980–2010). *Journal of Humanities and Social Science (IOSR-JHSS)*, 20(4), 115–123. DOI: 10.9790/0837-2045115123.

[11] Offodile, M.E. (2002): *Ground water study and development in Nigeria*. 2nd edition. Jos: Mecon geology and engineering services limited.

[12] Jayeoba, A., Oladunjoye, M.A. (2013): Hydro-geophysical evaluation of groundwater potential in hard rock terrain of southwestern Nigeria*. RMZ- Materials and Geo-environment*, 60, pp. 271–284.

[13] Akanbi, O.A. (2016): Use of vertical electrical geophysical method for spatial characterisation of groundwater potential of crystalline crust of Igboora area, southwestern Nigeria. *International Journal of Scientific and Research Publications,* 6(3), pp. 399–406.

[14] Meijerink, A.M.J. (2007): *Remote sensing applications to groundwater*. Paris: United Nations Educational Scientific and Cultural Organization (UNESCO).

[15] Shaban, A., Khawlie, M., Abdalla, C. (2006): Use of GIS and remote sensing to determine recharge potential zones; the case of occidental Linanon. *Hydrogeology Journal*, 14(4), pp. 433–443.

[16] Granados-Olivas, A., Corral Diaz, R. (2003): Fracture trace and alignment analysis for groundwater characterization. Hydrology of Mediterranean and Semiarid regions. IAHS Publ. 278 (Montpellier Symposium), pp. 24–28.

[17] Singhal, B.B.S., Gupta, R.P. (1999): *Applied hydrogeology of fractured rocks*. Dordrecht, Netherlands: Kluwer Academic Publishers; 400 p.

[18] Leblanc, M., Razack, M., Dagorne, D., Mofor, L., Jones, C., (2003): Application of Meteosat thermal data to map soil infiltrability in the central part of the Lake Chad Basin, Africa. *Geophysical Research Letter*, 30(19), Art. No. 1998.

[19] [19] Münch, Z., Conrad, J. (2007): Remote sensing and GIS based determination of groundwater dependent ecosystems in the Western Cape, South Africa. *Hydrogeology Journal*, 15 (1), pp. 9–28.

[20] Robinson, C.A., Werwer, A., El-Baz, F., El-Shazly, M., Fritch, T., Kusky, T. (2007): The Nubian aquifer in south-west Egypt. *Hydrogeology Journal*, 15(1), pp. 33–45.

Original scientific paper

Received: May 01, 2018
Accepted: Jun 08, 2018
DOI 10.2478/rmzmag-2018-0019

Improved neural network model of assessment for interpretation of miocene lithofacies in the Vukovar formation, Northern Croatia

Izboljšani nevronsko-mrežni model za oceno interpretacije miocenskega litofaciesa v Vukovarski formaciji v severni Hrvaški

Varenina Andrija[1], Malvić Tomislav[2], Mate Režić[3,*]

[1] Jabuka 9, 21240 Trilj

[2] University of Zagreb, Faculty of Mining, Geology and Petroleum Engineering, Pierottijeva 6, 10000 Zagreb, Croatia

[3] Stepinčeva 16, 21000 Split

* mate.rezic92@hotmail.com

Abstract

The Ladislavci Field (oil and gas reservoirs) is located 40 km from the city of Osijek, Croatia. The oil reservoir is in structural–stratigraphic trap and Miocene rocks of the Vukovar formation (informally named as El, F1a and F1b). The shallower gas reservoir is of Pliocene age, i.e. part of the Osijek sandstones (informally named as B). The oil reservoirs consist of limestones, breccias and conglomerates, and gas is accumulated in sandstones. Using neural networks, it was possible to interpret applicability of neural algorithm in well log analyses, and using neural model, it was possible to predict reservoir without or with small number of log data. Neural networks are trained on the data from two wells (A and B), collected from the interval starting with border of Sarmatian/Lower Pannonian (EL marker Rs7) to the well's bottom. The inputs were data from spontaneous potential (SP) and resistivity (R16 and R64) logs. They were used for neural training and validation as well as for final prediction of lithological composition in the analysed field. The multilayer perceptron (MLP) network had been selected as the most appropriate.

Key words: neural networks, Ladislavci Field, Drava Depression, Miocene, Croatia.

Povzetek

Naftno in plinsko polje Ladislavci je oddaljeno 40 km od mesta Osijeka na Hrvaškem. Naftni rezervoar je v strukturno-stratigrafski pasti v miocenskih plasteh Vukovarske formacije (delovne oznake El, F1a in F1b). Plitvejši plinski rezervoar je pliocenske starosti, v delu osjeških peščenjakov (delovna oznaka B). Plinski rezervoar sestoji iz apnencev, breč in konglomeratov, plin je pa nakopičen v peščenjakih. Z uporabo metode nevronskih mrež smo preverili uporabnost nevronskega algoritma za analizo karotažnih podatkov iz vrtin in nevronskega modela za napovedovanje rezervoarjev na osnovi majhnega števila podatkov ali celo brez njih. Učenje nevronskih mrež smo izvedli s podatki iz dveh vrtin (A in B), posnetimi v intervalu od meje sarmata s spodnjim panonom (EL reper Rs7) do dna teh dveh vrtin. Uporabili smo meritve lastnega potenciala (SP) in električne upornosti (R16 in R64). S temi podatki smo izvedli nevronsko učenje, validacijo in končno napovedovanje litološke sestave proučevanega polja. Kot najprimernejšo smo izbrali večslojno perceptronsko mrežo (MLP).

Ključne besede: nevronske mreže, polje Ladislavci, Dravska udorina, miocen, Hrvaška.

Introduction

Ladislavci Field (Figure 1) is located in the eastern part of the Drava Depression in the Croatian part of the Pannonian Basin System, 40 km east of Osijek, Northern Croatia. This area is predominantly a lowland with an average altitude of about 100 m. The eastern part of the Drava Depression is margined with mountains of Papuk and Krndija in the south, mostly with Drava river in the north, Mura Depression in the west and Slavonian-Srijem Depression in the east. Hydrocarbon research in this area began after geological interpretation of geophysical data collected in 1959, and the well Kučanci – 1 was constructed. The seismic sections recorded until 1973 provided better quality data on which the geological and economic basis for the project of the Ladislavci and the Kučanci structures was made. Two artificial neural networks are designed to predict wider reservoir lithofacies in the analysed field. Such lithofacies belong to the oldest Upper Miocene (Lower Pannonian) and Middle Miocene (Badenian, Sarmatian) lithofacies, i.e. lithostratigraphically had been analysed interval between e-log (EL) marker Rs7 (border between Lower and Upper Pannonian) and well bottoms. Analysed data had been transferred into categorical variable, derived from multi-log lithological analysis. Neural model had been programmed using "JustNN" program, fed by lithofacies data and reservoir depths. The analyses had been done for two wells, here named A and B. The network with a feedback procedure and several hidden layers, i.e. multilayer perceptron (MLP) network, was used. It was proved to be most successful in predicting Miocene lithofacies in the Ladislavci Field.

Basic hydrocarbon geology settings of the Ladislavci Field

The oil reservoir of the Ladislavci Field is of Miocene age (the Vukovar Formation) and gas (the Osijek sandstones) is of Pliocene age (Figure 2). The oil reservoir is divided into three informal units (El, F1a and F1b) [2], combined into structural–stratigraphic trap. According to Brod and Jeremenko [3] classification, it is a massive type reservoir in erosional buried hills. The reservoir rocks include limestone breccias, clastic limestones and breccias–conglom-

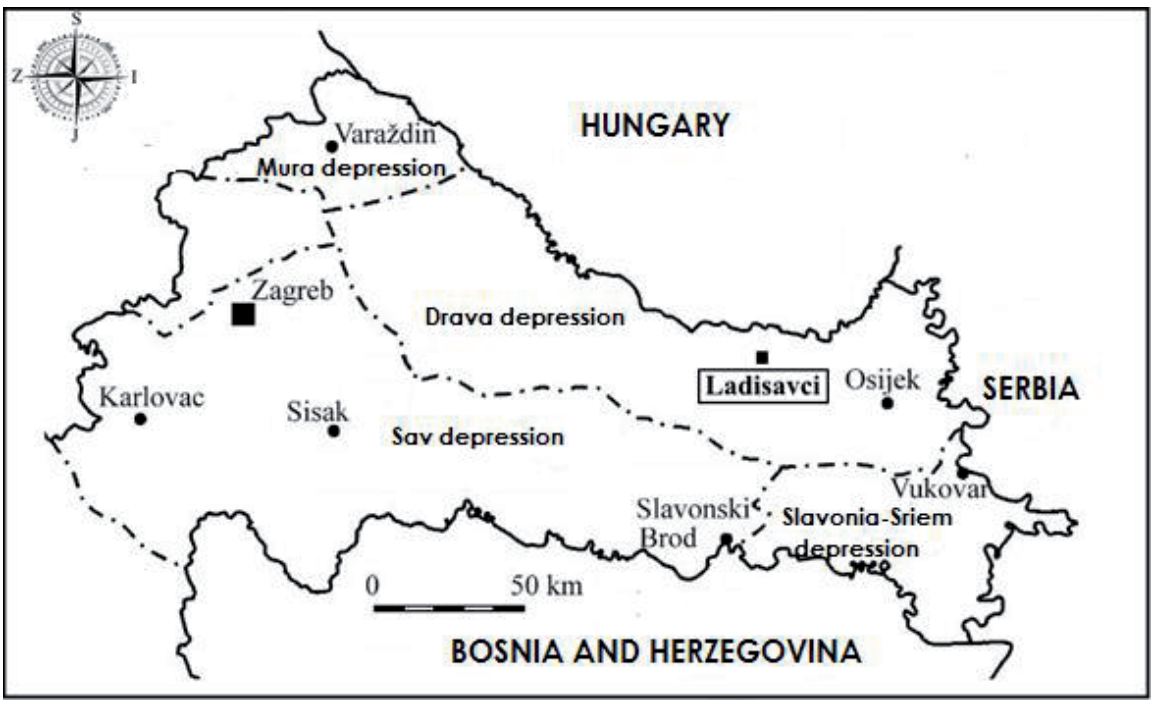

Figure 1. *The Ladislavci Field location in the Drava Depression (Northern Croatia) [1].*

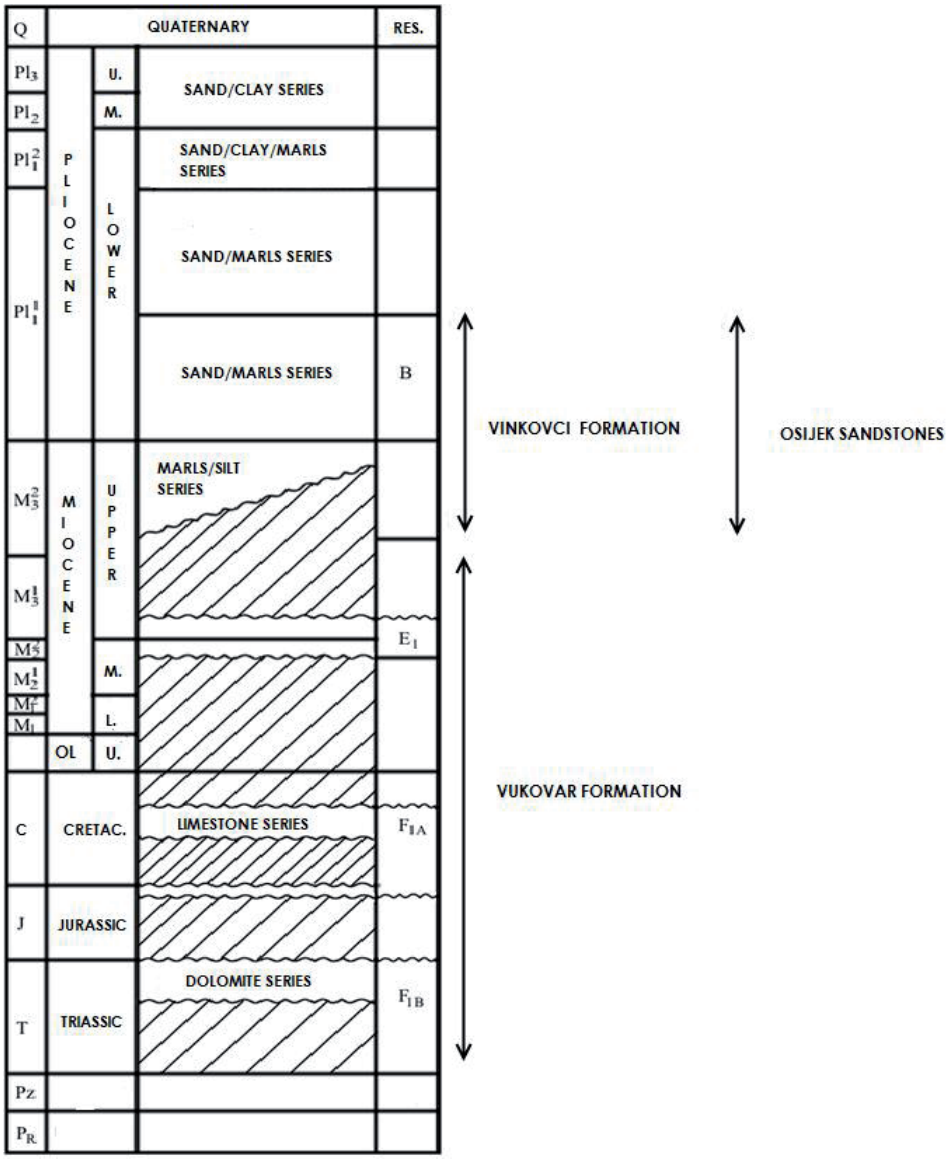

Figure 2. *The Ladislavci Field's stratigraphic column.*

erates. The secondary porosity varies considerably even at smaller intervals. From 6 wells that drilled reservoir rocks approximately at the same structural height, only 3 discovered rocks saturated with hydrocarbons. This was indication of locally weakly permeable isolator rocks inside the Ladislavci structure. Moreover, the reservoir fault zones represented barriers during hydrocarbon migration. Frequent vertical and lateral changes in lithofacies made reservoir development very difficult. Tectonic block is the reason why oil/water contact in different wells is at different depths. This is particularly evident in well B where the oil/water contact is 60 m deeper than that in well A. So, this contact in well B is found at -2180 m, but in the northern block, the same contact varies between -2115 and -2130 m.

Theory and application of neuronal networks

The term "neural networks" has a double meaning. Traditionally, this term referred to a biological (natural) neuron network constructed of biological neurons that are connected to the peripheral or central nervous system. Neuron

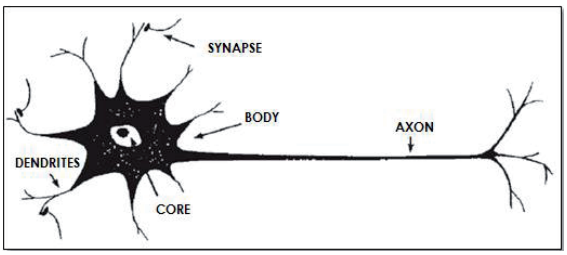

Figure 3. *Human neuron model [6].*

(the nerve cell) is a basic unit of the nervous system and is also the most complex unit of the human organism (Figure 3). Artificial neural networks have touch points with the human brain structure. It is common for both types of networks to transmit only two information, whether the connection is active or not, and these information are expressed by a certain electrical potential in the brain or computer. Similarity of these two networks is in the way these two states are used to make the final result as a simple processing of data. Both types of networks are based on repetitive procedures, iterations and exercises [4,5]. Artificial neural networks serve to understand biological neural networks and solve problems in the field of artificial intelligence (AI). They use the structure of the human brain to develop an appropriate data analysis strategy. Neural networks are widely used in social and technical sciences. In the following, it can be concluded that artificial neuron mimics the basic functions of biological neuron. The neural network is a set of mutually connected simple elements, units or nodes, whose functionality is based on the biological neuron. The power of analysis is to maintain the link between individual neurons, i.e. the difficulties that come from the adaptation process or by learning from the data set. The term AI is defined as any inactive system that has the ability to react in different and new situations.

Basic properties of artificial neural networks and their division

The most important properties of artificial neural networks are:

- Data processing that is distributed parallelly: Unlike conventional computing techniques, neural networks accept multiple inputs in parallel and receive processed data in a distributed manner. The data stored in the artificial neural network are distributed to multiple computing units, which are completely in opposite to conventional data storage where each particular datum/information is stored in its own storage space. The attribute of distributed data storage gives neural networks more advantages, the most important of which being redundancy, that is, the resistance to fail, and therefore, an artificial neural network will continue to work even if some of its parts are malfunctioned.
- Learning and adaptation: The ability to learn and adapt makes neural networks capable of treating inaccurate and badly kept data in an unstructured and indefinite environment. If certain data come in network's input and the same data are not from the sample on which the network is created and based, a properly trained neural network has the ability to amplify that certain data.
- Universal approximator: The most important feature of neural networks from the point of view of modelling, identification and management of nonlinear processes is that they approximate the continuous nonlinear function to the desired accuracy.
- Multivariable systems: Neural networks are multivariable systems, and this makes them easy to apply for modelling, identification and management of multivariable processes.
- Gate implementation: More than one manufacturer has developed specialised networking systems for neural networks, which allows parallel distributed processing in real time.
- Computationally demanding neural networks: The output of each neuron is the result of sum of more products of multiplying and calculation of the nonlinear activation functions.
- The calculation speed of the neural network is determined by the number of mathematical operations of a single layer rather than the entire network: Furthermore, each layer of the network has a parallel texture, i.e. each neuron in the layer can be viewed as a local processor parallel to other neurons.

- Neural networks require a large storage space: Each individual neuron has more synaptic links, each of which is associated with a weight coefficient that must be stored in memory. By increasing the number of neurons in the network, the memory requirements increase with the square of the number of neurons.

Neurons connected to the network are organised into layers. Each network has neurons that serve to accept the input values and make the input layer of the neurons and give the network response and make the output layer of neurons. All other neurons that lie between these two layers form a hidden neuron layer (e.g. [7]). Neural networks can be single- and multi-layered. One layer network consists of one layer of neuron (output layer), while the input layer is not counted because it does not have data processing. Multilayer networks have also one or more hidden layers of neurons (e.g. [8]). The main task of the network is to learn the model of the environment in which it will work and maintain the model accurate to achieve the desired goals of the given system. Learning is a process by which free parameters of neural networks are adapted through a continuous stimulation from the environment in which the network is located (e.g. [8]). A set of rules to solve a learning problem is called a learning algorithm, which determines the way to calculate changes in synaptic weight at the time (moment, n), while the learning paradigm (learning under supervision, learning by support, learning without supervision) determines the neural network's relation to the environment (e.g. [8]). For supervised learning, training data consist of examples with known input and output values. The network generates output, accounts for a mistake (the difference between the desired and the gained values) and adjusts the synaptic weight with respect to the error. The process is repeated iteratively until the network learns to imitate the exact model. In some situations, it is not possible to provide such information or data but only data that tell whether the output value is desirable or not. This type of learning is called "reinforcement". In this kind of learning, there is no validation data set that determines what is a mistake for certain input and output values, but it is known how much a particular learning step is good. Learning Support solves the problem of learning under supervision, that is, without a validation data set, the network cannot learn new strategies that are not covered by the examples used for learning. In unsupervised learning, output values are not known. Inputs are available in the network, and weights are not based on actual output values. Here, the artificial neural network organises itself, so the networks taught by this method are called self-organising neural networks. If the neuron layers are connected so that the signals travel in one direction from the input to the network outlet, such a network type is called the acyclic neuron network. If there is at least one feedback link, the network is called a reverse link network. By type, the neuronal linkage can be realised between two layers (between layers) and between neurons in one layer (interspersed). When a neuron receives the input from the previous layer, the value of its input is calculated by the input function, usually called a "summation" function. Activation functions are used to reduce the number of iterations. Consequently, neural networks can be divided into four main types (e.g. [7]): acyclic network, feedback network, side-by-side network and hybrid network.

Basic mathematical expressions of neural networks and working principle of artificial neural network

The output of each neuron represents the input signal modified by the corresponding function. Neuron output "j" is described in the following equations (e.g. [1]):

$$U_j = \Sigma \pm X_i w_{ij} \quad (1)$$

$$Y_j = F_{th} (U_j + t_j) \quad (2)$$

where j is the number of neurons, i the number of inputs, X_i the value of "i" input, w_{ij} the predetermined weight coefficient for input "i", U_j the common value of the output of all inputs "j", F_{th} the activation function and Y_j the output of the observed layer or the total output of the network.

When the common value U_j is computed, it is compared to the value to the threshold value

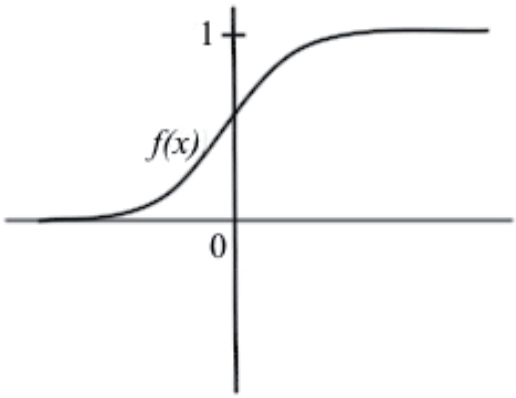

Figure 4. *Sigmoidal activation function.*

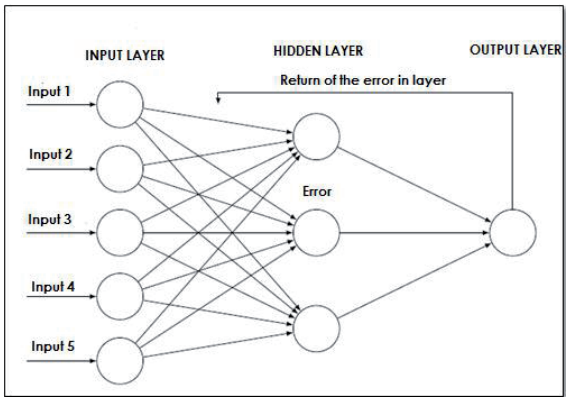

Figure 5. *MLP network scheme.*

(cut-off), i.e. the activation function F_{th} is tested. The term (1) represents a set of operations in the neuron and the other (2) examines whether this same neuron is activated.

The most common form of activation function is the sigmoidal (logistic) function. In addition to sigmoidal activation functions (Figure 4), other forms of activation functions may also be used. Sigmoidal function is defined by equation (3) (e.g. [1]) where parameter "a" determines the slope of the function:

$$f(x) = 1/(1 + e \wedge (- ax)) \quad (3)$$

The work of artificial neural networks can be divided into degree of learning (training), selection phase (cross validation), check phase and operational phase (degree of revocation). Two basic stages in the work of artificial neural networks are degree of training and the degree of verification. In the selection phase, the network tries to optimise the length of the training and the number of hidden neurons, after which the resulting network is stored and tested. The operational phase refers to the application of the neural network in new cases with unknown results but fixed weights. Prior to learning, it is necessary to prepare input data to which the network will be applied and define the model of artificial neural network. Data are usually divided into two sets, one is used to train the network, while the other is used for testing. It is recommended that the data set used for network training is 80% of input data and the remaining 20% of data are used for verification [9]. Learning is the process of adjusting weights in the network that takes place in multiple repetitions (iterations). The number of repetitions usually amounts to several thousands, and if it is possible to determine the difference between the actual and desired network response, the amount of error can be returned back to the network to minimise. This process is called a "backpropagation network" (Figure 5) and is repeated so many times until the single or total error drops below the desired value. The second work stage of the network is the testing of the same being carried out so that the network presents new input values that have not participated in the network learning process and generates the corresponding output values for the input values presented. Network evaluation is done by comparing the network's output value with the actual output value based on which error is calculated. The network no longer learns and does not expand its capabilities but only counts new values from the established amounts. The design process of artificial neural networks consists of several steps:

- defining the model (determining input and output variables);
- choosing the most suitable algorithm;
- putting neurons into layers;
- determining the type of connection between the neurons;
- determining layer functions;
- selection of training rules;
- selection of benchmarks for network assessment and
- performing a training session.

Geophysical methods used in analysis of Miocene lithofacies

Geophysical methods in selected wells include measurements of electrical resistance and spontaneous potentials (SPs; conventional electric logging) for the purpose of determining their porosity or saturation. Logging measurements were performed at the end of the 70s and 80s of the last century. This included the recording of SP values and electrical resistance with electrodes normally at a distance of 16″(R16) and 64″ (R64).

First application of neural networks at Northern Croatia hydrocarbon reservoirs – the Okoli Field

This network was base for developing neural analysis in the Ladislavci Field. The network was trained on the data obtained by interpreting the e-logs (GR, R16, R64, porosity, SAND and SHALE portion) from two wells (B-1 and B-2), which drilled Miocene reservoir "c" and Pliocene "c2". From the well B-1, GR curves (curves of natural radioactivity), R16 (resistance curve – "low normal" curves) and R64 (resistance curve – "normal" curves) were used. The input curves in the B-2 well were GR, PORE (effective porosity), PORT (total porosity), PORW (porosity in the part saturated with 100% water), R16, SANDSTONE (sand portion) and SHALE (marl portion). The output curve was called a "reservoir", and it represented a "categorised" variable, defined numerically with 0 and 1. Number 0 represented marl, and number 1 represented sandstone. For learning the network, 153 data with value 0 and 142 data with value 1 from the well B-1 were used in total. For validation (V), 48 data with value 0 and 50 data with value 1 were used. Network training performances are given in Table 1. The best network was marked with a total of 31,515 iterations and a learning time of 5.40 minutes and an average learning error of 0.00173 [9]. Simultaneous training and prediction were done in the B-2.

For the learning of the network (L – learning), 225 data were used with a value of 0 and 215 data were used with a value of 1. For validation (V – validation), 71 data had value of 0 and 75 data had value of 1; therefore, 586 data from which each tenth is shown in Table 2.

Table 1. *Probability of success of learning of network in well B-1 [10].*

Legend: 1) Data Type, 2) "Reservoir" Variable, 3) Probability of successful prediction								
L	0	78,3	V	1	78,3	L	0	78,3
L	0	78,3	L	1	78,3	V	0	78,3
L	0	78,3	L	1	78,3	L	0	78,3
L	0	78,3	L	1	78,3	L	0	78,3
V	0	82,1	L	1	78,3	L	0	78,3
L	0	78,3	L	1	78,3	V	0	78,3
V	0	82,1	L	1	78,3	V	0	78,3
L	0	78,3	L	1	78,3	L	0	78,3
L	0	78,3	L	1	78,3	L	0	78,3
V	1	82,1	L	1	78,3	L	0	78,3
L	1	78,3	L	1	78,3	L	0	78,3

Table 2. *Probability of success of learning of network in well B-1 [10].*

Legend: 1) Data Type, 2) "Reservoir" Variable, 3) Probability of successful prediction								
L	0	82,1	L	1	82,1	L	0	82,1
L	0	82,1	L	1	82,1	L	0	82,1
L	0	82,1	L	1	82,1	L	0	82,1
L	0	82,1	L	1	82,1	V	0	88,1
V	0	88,1	L	1	82,1	L	0	82,1
L	0	82,1	L	1	82,1	V	0	88,1
V	0	88,1	L	1	82,1	V	0	88,1
L	0	82,1	L	1	82,1	L	0	82,1
L	0	88,1	V	1	88,1	L	0	82,1
V	0	82,1	L	1	82,1	L	0	82,1
L	1	82,1	L	1	82,1	L	0	82,1
L	1	82,1	L	1	82,1	L	0	82,1
V	1	88,1	V	1	88,1	L	0	82,1
L	1	82,1	V	1	88,1	L	0	82,1
V	1	88,1	L	1	82,1	V	0	88,1
L	1	82,1	L	1	82,1	L	0	82,1
L	1	82,1	L	1	82,1	L	0	88,1
L	1	82,1	L	1	82,1	-	-	-
L	1	82,1	V	0	88,1	-	-	-
L	1	82,1	L	0	82,1	-	-	-
L	1	82,1	V	0	88,1	-	-	-

The B-2 network was programmed to 28,599 iterations, and an average learning error of 0.002681 was obtained. The obtained values were similar to those for the B-1 well but due to the higher number of logs, the total time of training of the network was longer by about 3 times or 16.13 minutes [9]. An overview of the results obtained from the data from the well B-2 shows that the predicted and actual values have a much smaller degree of correlation. According to the facies, the prediction of 1 (or sandstone facies) is 100%. On contrary, marl (value 0) is significantly underestimated with probability of only 7.8% for correct foreseen. Numerically, of the 296 input cells described as a marl, the value 0 is correctly predicted in 23 cases and replaced by the number 1 in 273 cases. If the results obtained from the B-1 borehole are observed, a similar appearance of a marl layer replaced with sandstone can be seen. The answer lies in the type and number of used logging curves (GR, R16, R64), i.e. introducing of SP or porosity logs could improve correct distinguishing of Neogene sandstones and marls [9].

Analysis of the Ladislavci Field lithofacies using artificial neural networks

For facies analysis in the Ladislavci Field, the "JustNN" program was used, and the input data were determined by the interpretation of e-logs from wells A and B. The program can very easily load data and create a multilayer neural network. After the training, the program weighted parameters that most affected the output. The neural networks were trained at a certain depth interval. The program stopped training if the default error was reached or recorded the iteration in which the lowest selection error has been reached.

Prediction of the lithology

For the purpose of predicting the lithological composition, the reservoir (limestone breccia, clastic limestone and breccia/conglomerates) and isolator rocks (limonitised mudstone) were routinely separated from the boreholes A and B by logging diagrams. These were separated on the basis of the difference between the pass-through intervals of the permeable and nonpermeable rocks according to the position of inflection points on the SP curve. The most successful were those networks where half of the input data were used for training, while the other half were used to check the performance of the network. For the well A, network was trained on data from the range of -2153 to -2228 m and the prediction of the lithology was done from -2228 m to -2282 m. For the well B, the network was trained on data in the interval from -2122 to -2224 m, while the prediction of the lithology was made from -2224 m to -2327 m.

Analysis in the well A

The values of SP (Figure 6), resistivity (R16 and R64) and interpreted lithology were used. The analysis included 130 data, of which 66 were with a value of 1 and 64 were with a value of 0. Number 0 represents limonitised mudstone, and number 1 limestone breccia, clastic limestone and breccias–conglomerates.

The network that proved to be the most successful in training and predicting Miocene lithofacies in the well B was a reverse-feedback network (part of the MLP) with four neurons in the first hidden layer, one neuron in the sec-

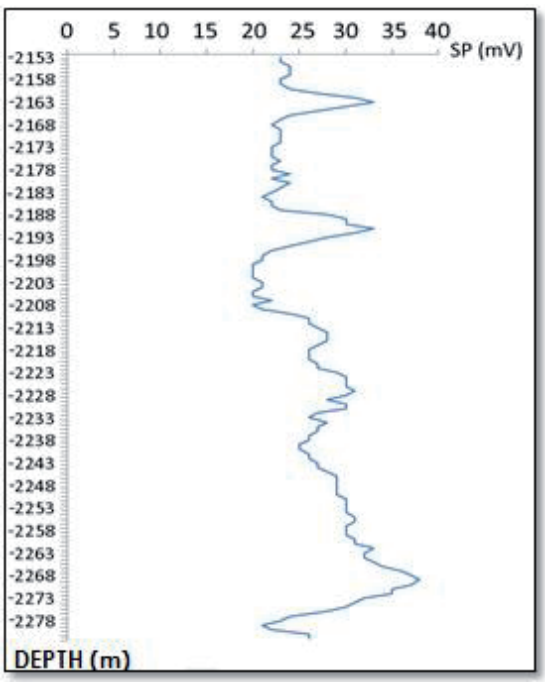

Figure 6. *Values of spontaneous potential in the well A.*

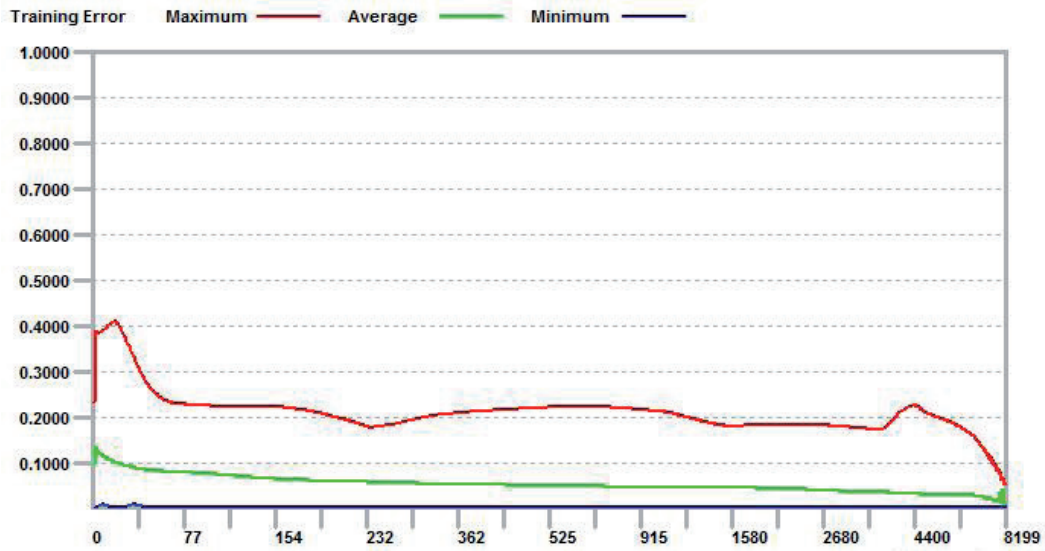

Figure 7. *Learning of the neural network in the well A (y-axis represents error values and x-axis represents number of iterations. The red line represents the largest, the green line represents the average and the blue line represents the lowest error of the training.).*

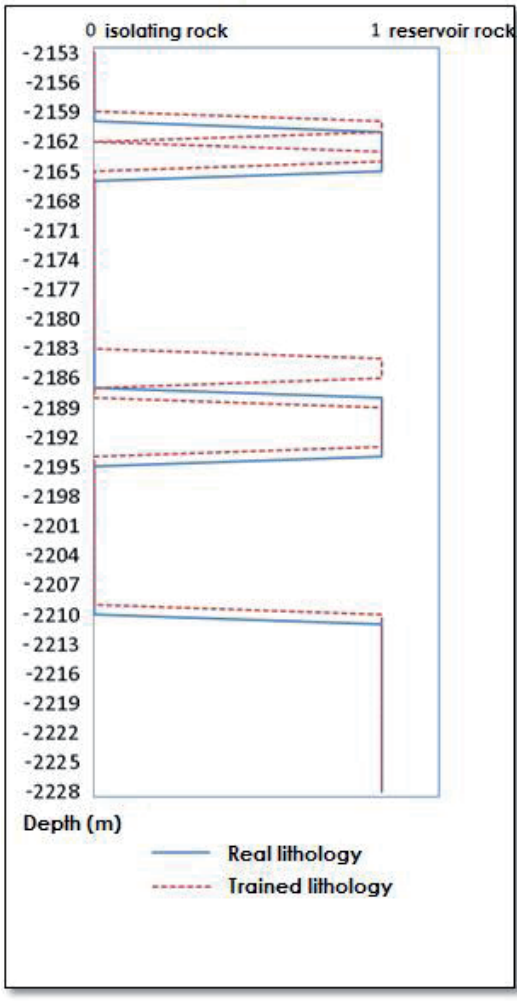

Figure 8. *Training MLP network on data from the well A.*

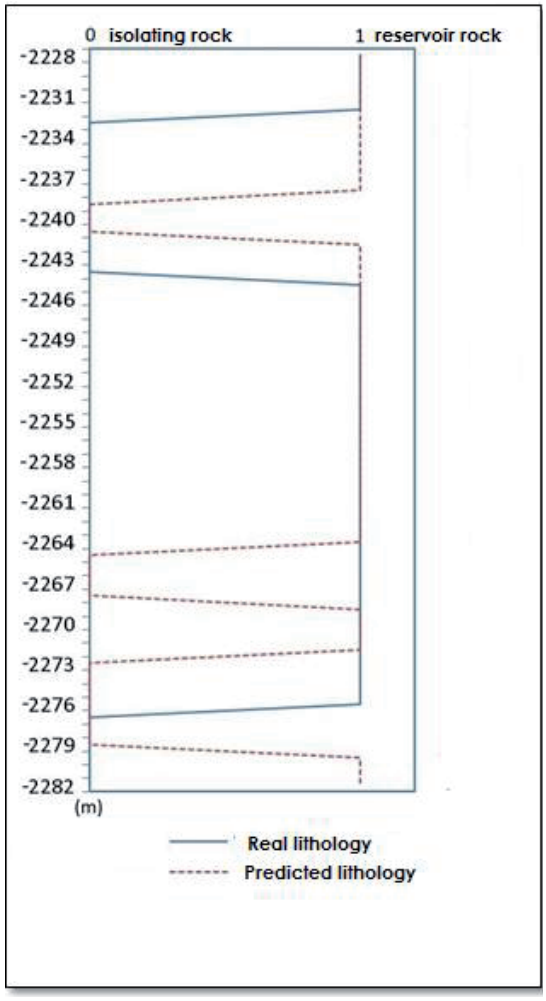

Figure 9. *MLP network prediction in well A.*

ond hidden layer and two in the third hidden layer (Figure 7), including 8199 iterations and an average error of 0.024865 (Figure 8). The network set is divided so that one half is used for training and the other half is used for validation. The SP log was the most important network variable.

The network was trained at a range of -2153 to -2228 m. For the training, 65 data were used. According to the error, it can be concluded that the network is rather poorly trained and has not successfully determined the layer boundaries. It could be explained by a small number of input data. From Figure 9, it is apparent that the network replaced non-permeable layers with permeable layers in the range of -2183 m to -2187 m.

To determine the network performance in well A, 65 data were used. From Figure 10, it is apparent that the results are bad and that the network has not successfully determined the layer boundaries and lithological composition.

Analysis in the well B

Data used for training of artificial neural network were the values of SP (Figure 11), resistivity (R16 and R64) and the lithological composition. The input data were taken from the depth of the EK marker Rs7 (-2122 m) to the bottom of the well (-2327 m), each 1 m. Total of 205 data were analysed, of which 77 were with a value of 1 and 128 with 0. The number 0 represented limonitised claystone, and the number 1 represented limestone breccia, clastic limestone and breccia–conglomerates.

The most successful network in training and predicting Miocene lithofacies in the well B was a reverse-feedback network (type of MLP) with four neurons in the first hidden layer, five in the second hidden layer and two in the third hidden layer (Figure 12) and was marked with a total of 15,658 iterations and an average error of 0.016835 (Figure 13). The network training data set was divided so that one half of the set was used for training and the other half was used for determining network performance.

The network is trained at an interval of -2122 m to -2224 m with 103 input data. Although the amount of error is smaller than that in the previous analysis, it can be seen that the network has not successfully predicted the boundary

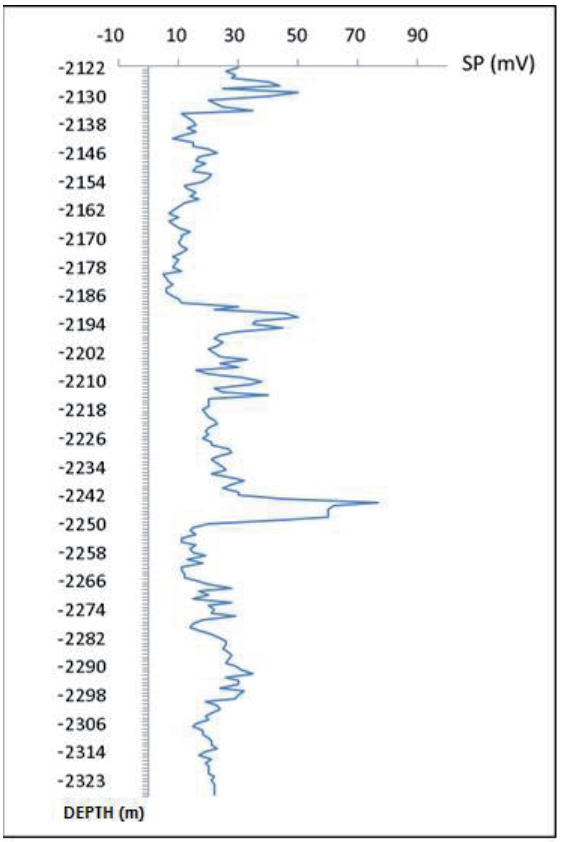

Figure 10. *Values of spontaneous potential for well A.*

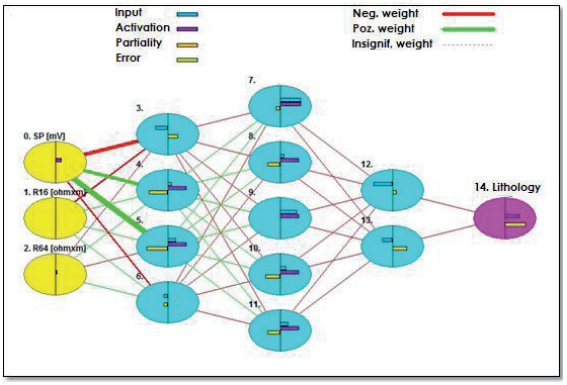

Figure 11. *Architecture of artificial neural network used for the prediction of Miocene lithofacies in the well B.*

of the layers. It is explained by the size of the input data set and the frequent vertical and lateral changes in the reservoir rocks of the Ladislavci Field. Network learning could be probably largely improved with GR log and calliper.

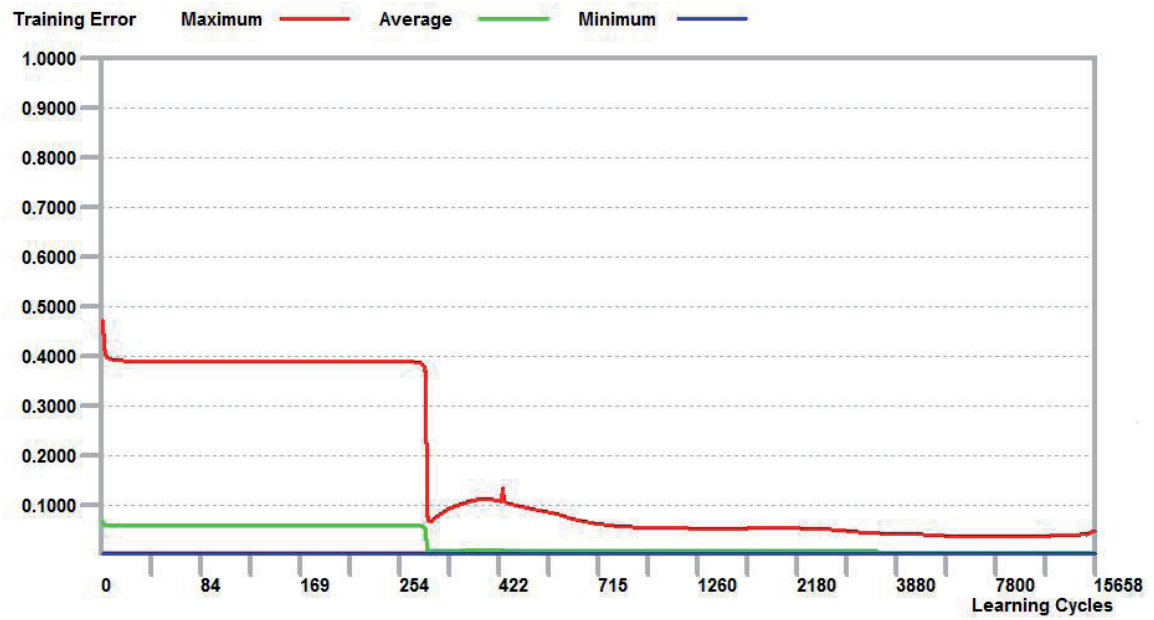

Figure 12. *Learning of the neural network in the well A (y-axis represents error values and x-axis represents number of iterations. The red line represents the largest, green line represents the average and the blue line represents the lowest error of the training).*

Conclusion

Two artificial nerve networks were constructed with feedback procedure and several hidden layers. These MLP networks had been used for prediction of the Miocene lithofacies in the Ladislavci Field. The data sets were divided so that one half is used for training and the other half for is used for validation of the network. The network that proved to be the most successful in the training and prediction of Miocene lithofacies was a network with feedback information (MLP). In the well A, it had four neurons in the first hidden layer, one in the second hidden layer and two in the third hidden layer. In the well B, the most successful was the network with four neurons in the first hidden layer, five in the second hidden layer and two in the third hidden layer. The main results and recommendations are as follows:

- The SP log is the most important parameter through which the neural network was used for prediction of lithology and has about 3 times greater relative importance in relation to the R16 and R64 logs during network training.
- Networks had not successfully determined layer boundaries, which can be explained by a small number of input data and a complex reservoir lithology.
- The frequent vertical and lateral changes in the reservoir rocks of the Ladislavci Field made training and prediction difficult.
- In the well A, the network replaced the impermeable layers in the range of -2183 to -2187 m.
- In the well B, the network replaced impermeable sections in the range of -2197 to -2209 m.
- The probability of successful prediction of lithofacies in the well A was 61.5% and in the well B was 63.1%.
- In the well A, an actual and predicted position of limonitised claystone was matched with 46.6% and limestone breccia was matched with 673%.
- In the well B, limonitised claystone was matched with 63.1% and limestone breccia was matched with 58.18%.
- To obtain better results for lithological prediction, it was recommended to use GR log (natural radioactivity), calliper, compensated neutron (CN) density and density (DEN) log.

Although the results do not indicate full potential of neural networks in petroleum exploration, they are a useful tool. The problem noted here is a small thickness of individual reservoir units and consequently a small number of input data, so the error is relatively large. Another problem is that reservoirs are heterogeneous. Because of this, logs are not developed as theoretical ones. The analysis had shown that this type of network can be used in the Ladislavci Field as an auxiliary tool at those intervals of deposits that are not logged in details or not logged at all.

Acknowledgment

This work is done by financial support from project "Mathematical methods in geology II" (head T. Malvić), funded by University of Zagreb, Faculty of Mining, Geology and Petroleum Engineering in 2017 (no. M048xSP17).

References

[1] Malvić, T., Cvetković, M. (2009): *Neuronski alati u geologiji ležišta ugljikovodika (Neural tools in geology of hydrocarbon reservoirs)*. Croatian geological society (Geomathematical section), manual, Zagreb: University of Zagreb, 100 p.

[2] Kosovec, Z. (1995): *O produktivnom kompleksu nafte na polju Ladislavci*, Sveučilište u Zagrebu (RGN fakultet), diplomski rad, Zagreb.

[3] Brod, I.O., Jeremenko, N.A. (1957): *Osnovi geologii niefti i gasa*. Moskva: Gostoptehizdat, 480 p.

[4] Rosenblatt, F. (1957): The perceptron: A perceiving and recognizing automaton. Project PARA, Cornell Aeronautical Lab, Technical report 85-460-1.

[5] Rosenblatt, F. (1958): The perceptron A probabilistic model for information storage and organization in the brain. *Psychological Review*, 65, pp. 386–408.

[6] Bolf, N., Jerbić, I. (2006): Primjena umjetnih neuronskih mreža pri identificiranju i vođenju procesa. Kemija u industriji (Application of artificial neural networks in identifying and managing the process. *Chemistry in industry*, 55(11), pp. 457–466.

[7] Dalbelo-Bašić, B., Čupić, M., Šnajder, J. (2008): Umjetne neuronske mreže, nastavni materijali za kolegij Umjetna inteligencija (Artificial Neural Networks, teaching materials for the course Artificial intelligence). Fakultet elektrotehnike i računalstva Zagreb. Available on: <http://www.fer.hr/_download/repository/UmjetneNeuronskeMreze.pdf>

[8] LONČARIĆ, S: Predavanja (Lectures), Available on: <www.fer.unizg.hr/predmet/neumre_a/predavanja>

[9] Malvić, T. (2006): Clastic facies prediction using neural network (case study from Okoli field). *Nafta*, 57(10), pp. 415–431.

[10] Malvić, T., Cvetković, M. (2013): *Neuronski alati u geologiji ležišta ugljikovodika*, (Neural tools in geology of hydrocarbon reservoirs), 2nd edition, Croatian geological society (Geomathematical section); University of Zagreb, manual, Zagreb, 89 p.

Original scientific paper

Received: Jan 18, 2018
Accepted: Aug 14, 2018
DOI 10.2478/rmzmag-2018-0016

Obtaining a new kind of organic fertilizer on the basis of low-grade phosphorite of Central Kyzylkum

Pridobivanje nove vrste organskega gnojila na osnovi nizkoprocentnega fosforita iz osrednjega Kizilkuma v Uzbekistanu

Nodirjon Abdihakimovich Doniyarov*, Ilkhom Ahrorovich Tagayev
[1] Navoi State Mining Institute, Navoi, Uzbekistan
* intelekt_16@mail.ru

Abstract

The paper presents the results of processing low-grade phosphorites by microorganisms of activated sludge from the biochemical purification production unit of JSC "Navoiazot". The obtained results on the leaching of rare and rare-earth elements into the liquid phase make it possible to separate them and thus enrich the phosphorites. Other options are the gravitational separation of the crushed calcite particles. In addition to this, there is a real possibility of creating complex organomineral fertilisers.

Key words: activated sludge, organomineral fertilisers, phosphorite flour, fluorapatite, francolite

Povzetek

V članku so predstavljeni rezultati obdelave nizkoprocentnih fosforitov z mikroorganizme vsebujočim aktivnim blatom iz proizvodne enote za biokemijsko prečiščevanje Delniške družbe "Navoiazot". Rezultati izluževanja redkih in redkozemeljskih prvin v tekočo fazo kažejo, da jih je mogoče ločevati in tako fosforite bogatiti. Nadaljnja možnost je težnostno ločevanje drobcev kalcita. Razen tega se kaže obetavna tudi možnost pridobivanja kompleksnih organskomineralnih gnojil.

Ključne besedes: aktivno blato, organskomineralna gnojila, fosforitna moka, fluorapatit, francolit

Introduction

Uzbekistan, being an agro-industrial country, occupies 3.73 million hectares of irrigated arable land. It produces 97% of the country's agricultural output.

It turns out that we have only 39.8 kg of P_2O_5 per hectare of irrigated arable land, while it is necessary to insert for growing grain crops 100–120 kg/ha P_2O_5, cotton 145–165 kg/ha P_2O_5, vegetable crops 100–110 kg/ha P_2O_5, rice 140–145 kg/ha P_2O_5 and maize for grain 120-140 kg/ha P_2O_5. This indicates that our agricultural production is experiencing a large deficit in phosphorus fertilisers. Deficiency of phosphorus fertilisers is further aggravated by the fact that a large number of nutrient components are removed from the soil with the crop. It is known that one ton of raw cotton takes out 45 kg of nitrogen, 15 kg of P_2O_5 and 45 kg of K_2O from the soil annually. One ton of wheat takes out 35 kg of nitrogen, 10 kg of P_2O_5 and 24 kg of K_2O from the soil every year. With a gross harvest of 3 million tons of raw cotton and 6.1 million tons of wheat, only 348,500 tons of nitrogen, 106,000 tons of phosphorus and 281,400 tons of potassium are lost annually from these two crops. However, other cultures also carry a large amount of nutrients out of the soil. It should be noted that the production of phosphorus-containing fertilisers in the Republic is limited by the quality of the phosphorite of the Central Kyzylkum field. It is a phosphorus-poor raw material, which also contains a large amount of undesirable impurities, in particular, carbonates and chlorine. Such a raw material is not suitable for obtaining highly concentrated phosphorus-containing fertilisers; in other words, it is not suitable for nitric, sulphuric and hydrochloric acid processing into concentrated phosphorus-containing fertilisers. A large amount of acid will be spent not on decomposition of fluorapatite but on interaction with calcium carbonate, giving large-scale waste products such as nitrate, sulphate and calcium chloride. Acid processing of such highly carbonised raw materials is accompanied by abundant foaming, which largely violates the whole technological process and reduces the productivity of equipment. To get a high-quality phosphorus fertiliser from such raw materials, they must be pre-enriched.

Therefore, the Kyzylkum Phosphorite Plant (KFP) carried out multi-stage enrichment: crushing, dry enrichment to obtain ordinary phosphorite flour, washing away from chlorine and roasting to remove CO_2. At present, KFP produces three types of phosphate raw materials using the method of thermal treatment at a temperature of 1200°C: washed burned concentrate (P_2O_5 – 27–29%, C1 <0.04%) in the volume of 400 thousand tons per year, washed dried concentrate (P_2O_5 – 18–19%) in the amount of 200 thousand tons per year and ordinary phosphorite flour (P_2O_5 – 16-18%) in the amount of 200 thousand tons per year. The availability of phosphorus fertilisers for the Republic's agriculture is only 29–30%. The situation is aggravated also by the fact that the coefficient of phosphorus utilisation by plants from phosphorus fertilisers introduced into the soil is extremely low and does not exceed 20%. The rest of the phosphorus is fixated on the soil and shows a slight effect already in the after-effect [1].

The vast majority of ores in their natural form do not meet the requirements of either P_2O_5 or the amount of harmful impurities. Therefore, one more important stage – enrichment – is included in the general scheme for processing phosphorite ores. Its essence consists of concentrating by various mechanical methods of a useful mineral and removing harmful and ballast impurities in the tail (tails). Enrichment is based on the features of the structure and the difference in the properties of ore minerals. The methods used in the enrichment of phosphorites are the same as those used in metallurgy. A large number of methods are given, among which are used the following: ore disintegration, enrichment by size, gravity separation, flotation, roasting and selective removal of carbonates by different reagents [2]. The German company "KHD Humboldt Vedag AG" built and commissioned a factory for dry enrichment near the Khouribga deposit (Morocco). The regularities of flotation behaviour of minerals served as the basis for selective flotation of carbonate phosphorites of Karatau [3]. The technological scheme with the use of flotation enrichment methods is given in Cheryatu [4],

where the presence of a phosphate ion in the pulp enhances the difference in the properties of the dolomite and phosphate surfaces, providing dolomite flotation with fatty acids [5,6]. In an acidic environment, the collector is in a molecular form and to increase its dispersity. It is proposed to feed the flotation with fatty acids in combination with alkyl–acrylic sulphates. For example, after the firing process, the content of P_2O_5 in the calcined concentrate is 27 ± 1% [7,8].
In the scientific literature, numerous methods have been suggested for enriching poor phosphorite ore [11] with various gases (oxides SO_2 [9], NO and NO_2 [10]) and acids (HCl [11,12], H_2SO_4 [13,14], H_3PO_4 [15,16] and HNO_3 [17]).
The new method of biotechnological treatment that we applied is based on the ability of certain types of microorganisms under certain conditions to use pollutants as their food. A lot of microorganisms that make up the active sludge of the biological treatment plant, being in the waste liquid, absorb pollutants into the cell where they undergo the biochemical transformations under the influence of enzymes. In this case, organic and some types of inorganic pollutants are used by the bacterial cell in two ways:

1. Biological oxidation in the presence of oxygen into harmless products of carbon dioxide and water:
   Organic matter + O_2 (in the presence of enzymes) => $CO_2 + H_2O + Q$.
2. The energy released in this case is used by the cell to support its vital activities (movement, breathing, reproduction, etc.).
   Synthesis of a new cell (multiplication): Organic substance + N + P + Q (in the presence of enzymes) => new cell [18].

The aim of the studies was to study the possibility of microorganisms of active silt for their growth and development to use carbon carbonates in the composition of calcite.

Object and methods of research

The object of the study was the phosphorite ore of the Jeroy-Sardarinsky deposit with chemical composition given in Table 1.
In connection with the foregoing, there have been conducted laboratory studies on the leaching of various elements from low-grade phosphorites of the Jeroy-Sardarinsky deposit using aerobic species of neutrophil microorganisms of the active sludge of the biochemical purification station of JSC Navoiazot.
The microflora of activated sludge from the biochemical purification plant in the form of a liquid phase (L) was mixed with phosphorite (S – solid) in a ratio of L:S (liquid:solid) = 4:1. The experiments were carried out in several versions in reactors simulating aerotanks using water, activated sludge, activated sludge with nitrogen feed and compressed air supply with continuous mixing.
After bacterial leaching for 14 days, samples of the liquid and solid phases were sent to State Unitary Enterprise "Uzgeorangmetliti" for X-ray fluorescence energy-dispersive spectral

Table 1: *Chemical composition of phosphorites of Central Kyzylkum.*

No	Names of compounds	Content of elements, %	No	Names of compounds	Content of elements, %
1	P_2O_5	8.0–12.0	8	CO_2	8–15
2	Al_2O_3	1.5–3.0	9	Fluorine	1.8–3.2
3	SiO_2	6.0–8.0	10	SO_3	2.5–3.5
4	CaO	42–48.1	11	U	0.003–0.008
5	MgO	2.5–3.5	12	The amount of rare earth elements	0.04–0.089
6	Fe_2O_3	0.6–0.8	13	H_2O	10.0
7	SO_3	2.8–3.0	14	Insoluble residue	8.0–8.2

analysis performed using the BRA-135F instrument. The universal X-ray fluorescence energy dispersive spectrometer BRA-135F allows to simultaneously determine up to two dozens of chemical elements in a time not exceeding 300 seconds in a wide range of concentrations from hundreds of ppb. BRA-135F analyses the samples in solid, powdery, liquid states, as well as those deposited on the surface or on filters.
In order to determine the shape of phosphorite grains and calcite crystals, a conventional light microscope "Celestron" was used, where at an increase of 200 times, the production of not only conventional but also stereoscopic images were achieved, changing the angle of illumination (illumination was carried out from the surface part of the sample).

Results and discussion

Active sludge is a complex substance that participates in the sewage treatment process and is an amphoteric colloidal system. Biofilm is a collection of microorganisms located on the surface of sewage. The composition of activated sludge and biofilm directly depends on the chemical composition, temperature, pH and other characteristics of sewage from the sewerage of country houses and other residential objects.

Organic substances of activated sludge
Dry silt matter in septic tanks without pumping (autonomous sewage treatment plants) contains 70–90% of organic substances in living organisms. They are represented in 12 main types of protozoa and microorganisms. The main activators of the sludge are bacteria: in 1 m^3, the number of bacteria is up to $2 \cdot 10^{14}$. They form clusters, surrounded by mucus. Nitrosomonas, nitrobacter, bacillus and some other microorganisms live in the biocenosis of the sludge. They are absorbed by flagellar, sarcodic, sucking and ciliated infusoria, resulting in clarification and sedimentation of the silt. The listed microorganisms, in turn, feed on worms (rotifers, eolosomes). Active sludge and biofilm contain 10–30% of inorganic substances such as water, a substrate (solid residues to which microorganisms are attached) and an inorganic suspension. The processes of biological oxidation can take place only in the presence of water and a significant amount of oxygen, and reproduction can take place only with the participation of nitrogen and phosphorus. Active silt contains also trace elements (manganese, sulphur, cobalt, iron, etc.). The ecosystem of activated sludge is artificially created and depends on various factors of its environment. Therefore, the species inhabiting it, in terms of abundance and species diversity, differ significantly from those that exist in the natural environment. Those microorganisms that began to dominate in numbers among the rest, due to natural selection, associated with the peculiarities of the composition and properties of the nutrient medium of the aerotank, created by wastewater, have high adaptive properties, due to the conditions of their selective selection. In this biomass, there are colonies of bacteria and microorganisms that ensure the release of carbon, biogenic and other elements from waste water [18].
This process is carried out with the aerobic action of activated silt on phosphorites for 14 days. On the 4th–5th day, microscopic examination of phosphorites revealed a change in the morphological structure of phosphorite grains, where they turned from irregularly angular to round and spherical structure, with a parallel decrease in grain size. In the aerobic decomposition of effluents, two basic microbiological processes occur: oxidation of organic carbon and nitrification with the participation of filamentous, flocculating microorganisms and bacterial nitrifiers. Flocculating bacteria are responsible for the oxidation of organic compounds. These include microorganisms of the genera *Actinomyces*, *Alcaligenes*, *Bacillus*, *Cellulomonas*, *Desulfotomaculum*, *Flavobacterium*, *Mycobacterium*, *Nocardia*, *Pseudomonas*, *Sarcina* and others. The most numerous bacteria (up to 80 percent of the whole complex of microorganisms) are microorganisms of the genus *Pseudomonas*, capable of oxidising alcohols, paraffins, fatty acids, carbohydrates and aromatic hydrocarbons. It is known that species of the genus *Pseudomonas* are able to oxidise also cyanides. Carbon-oxidising filamentous microorganisms are represented by the genera *Spherotilus*, *Beggiatoa* and *Thiotrix*.

At the same time, these microorganisms are the main cause of poor sedimentation of sludge in the settler and the formation of a stable foam in the device. During purification of sinks with a high carbohydrate content and nitrogen deficiency, there is sometimes an intensive development of heterofermentative lactic acid bacteria of the genus *Leuconostoc*, which form a powerful dextran capsule, which hinders sedimentation of the sludge in the settler. The most active nitrification processes occur after the oxidation of the organic component. In sewage with sulphur content, sulphate reductors, thionic and sulphur bacteria develop. Thionic microorganisms develop under the condition that the reduced sulphur compounds are contained in the effluents.

In the absence of organic compounds in the composition of phosphorites, many species of microorganisms die. However, the characteristics of heterotrophic microorganisms are that they can adapt to any environmental conditions and, with a lack of organic compounds, are able to switch to inorganic compounds and oxidise them. Extracellular enzymes in active silt contain proteases, hydrolases, cellulases and peroxidases. Extracellular enzymes catalyze the oxidation of substrates with the participation of hydrogen peroxide and catalase, decomposing H_2O_2.

Phosphorites of the Kyzylkum are composed mainly of phosphatised faunal residues, bound with fine-grained calcite cement [19]. Among phosphatised remains of fauna, foraminifera prevails with sizes of shells from 0.04 to 0.5 mm. Isotropic and weakly crystallised phosphate with point inclusions of calcite fill the internal cavities of their shells. Relic calcite, preserved from phosphate substitution, sometimes also forms a shell and internal septa shells. In the scientific and technical literature, such a calcite, which is located inside the phosphate formations, is called the "endocalcite", and the cement composing the rock is called the "exocalcite". The third form of calcium carbonate is found in the form of a phosphate mineral isomorphically entering the crystal lattice.

The subordinate role is played by the phosphatised remains of other groups of organisms: valves and cores of pelecites, gastropod shells up to 5 mm in size and up to 5–10% in places, elongated cone-shaped pteropods up to 4–5 mm in length and up to 1.5 mm in diameter, needles of sea urchins, fish scales, etc. Cementation is often unstable; many phosphorites easily disintegrate under mechanical action, especially after soaking in water. Among organic residues, a small amount of primary phosphate material is present – teeth of sharks, vertebrae and small (several millimetres) fragments of bones of marine animals. The cement of phosphorites is fine-grained calcite with an admixture of clay and phosphate–clay material. In the terminal part of the second layer, the cement is a strong crystalline; it is represented by calcite and gypsum and sometimes with a siliceous component. The results of mineralogical study of granular phosphorite ores indicate a monotony of their composition. The main phosphate minerals – francolite (fluorocarbonatepatite) and calcite – compose 80–90% of the ore. Francolite contains on average about 42.1% P_2O_5, 55.4% CaO, 1.2% F, 2.3% Cl and 0.6% H_2O; the sum of rare elements (TR) reaches 0.03%. The ore of the deposit has the following average mineral composition (weight, %): francolite – 56.0, calcite – 26.5, quartz – 7.5–8.0, hydromica minerals and feldspars – 4.0–4.5, gypsum – 3.5, goethite – 1.0, zeolite < 1.0 and organic matter – about 0.5 [21,22].

It should be noted that the distinctive feature of the Kyzylkum phosphorites is their high degree of carbonate content; the concentration of CO_2 in some formations reaches 27% or more.

The obtained results confirmed the assumptions about bacterial leaching of various elements, in particular, strontium, thorium and uranium into the solution. In the variant with active silt, the amount of strontium and thorium leached into the solution was respectively 21.2 and 1.09 mg/l (adequately).

Spectral analysis of samples (spectral analyzes were conducted using X-ray fluorescent energy-dispersive spectrometer BRA-135F) treated with active silt showed that not only radioactive metals but also rare-earth metals were released into the liquid phase. In the solid phase, the amount of radioactive and rare-earth metals varied within different limits, proceeding from partial dissolution and isolation into the liquid phase. The greatest amount of uranium (7.97 mg/l) was leached in the version with the

Table 2: *Distribution of alkaline earth and radioactive metals in solid and liquid phases (mg/l).*

No	Variants	Solid phase								Liquid phase		
		Mo	Ni	Cu	Zn	As	Sr	Th	U	Sr	Th	U
1	Initial	0.000193	-0.00521	0.0026	0.01228	0.000918	510.521	3.2480	1.9065	–	–	–
2	Initial + H_2O	0.000247	-0.00385	-0.0008	0.01781	0.001421	683.448	7.2064	14.325	13.04	0.547	4.452
3	Alkaline initial + H_2O	0.000241	-0.00502	-0.0012	0.01444	0.001547	544.353	3.5165	0.5553	21.20	1.090	5.964
4	Alkaline initial + O_2 + + urea	0.000242	-0.00533	0.0057	0.0143	0.001296	545.482	4.468	5.3095	11.63	0.421	7.971

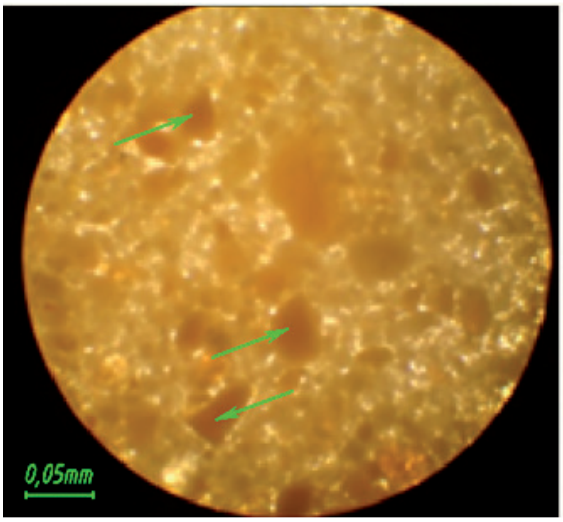

Figure 1: *Control variant (the scale is 20 × 10).*

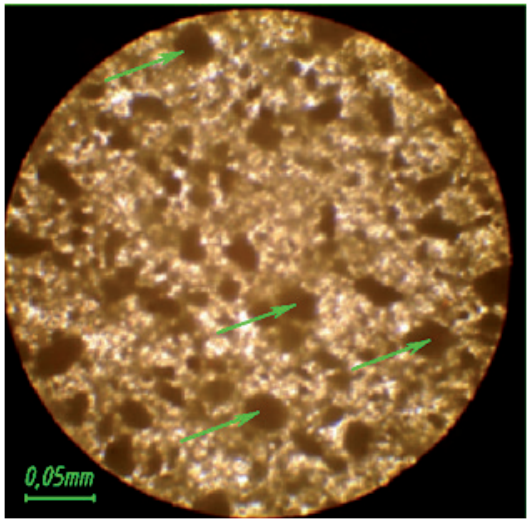

Figure 2: *Treatment with activated sludge (the scale is 20 × 10).*

use of activated sludge with air supply and using nitrogen fertilising in the form of urea. The behaviour of arsenic should be specially noted, which also underwent oxidation and passed into solution, especially in the third variant (Table 2).

The analysis under a microscope showed selective crushing of phosphorite ore. The obtained results show that, apparently, the microorganisms underwent destruction of the organic component of phosphorites, which is about 0.5%. In addition, incidentally, as a source of phosphorus, they used phosphorite grains (francolite), which in microscopic photos decreased in size and acquired a spherical shape.

In the control variant (Figure 1.), phosphorite grains are seen in fairly large sizes, up to 40–60 mm (shown by arrows). After processing the microflora of the activated sludge, the grains decreased in size to 20–35 mm (Figure 2), taking a round or spherical shape (indicated by arrows). When phosphorites with activated sludge were added to the nutrient mixture in the form of a nitrogen-containing fertiliser – carbamide and air aeration with the use of a compressor (Figure 3), the phosphorite grains further decreased in size to 5–15 mm. Phosphorite grains are represented mainly by francolite, which has a complex chemical composition, in which the phosphorus content reaches up to 40% and the endocalcite up to

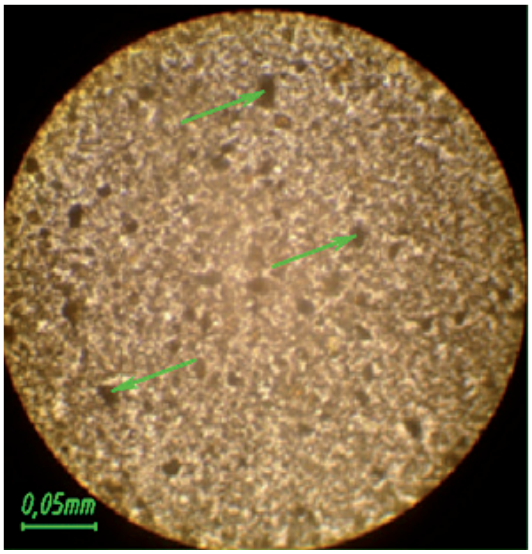

Figure 3: *Treatment with activated sludge, carbamide and air (the scale is 20× 10).*

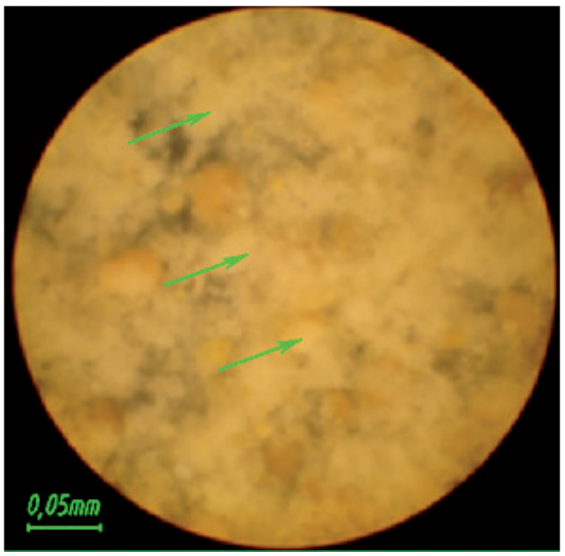

Figure 4: *Control variant (the scale is 20 × 10).*

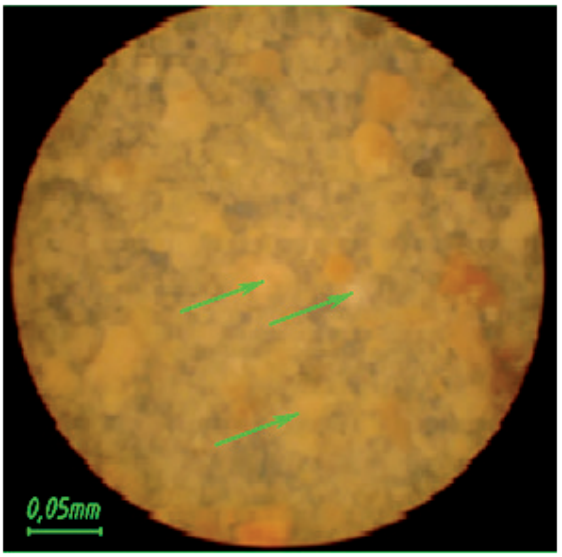

Figure 5: *Treatment with activated sludge (the scale is 20 × 10).*

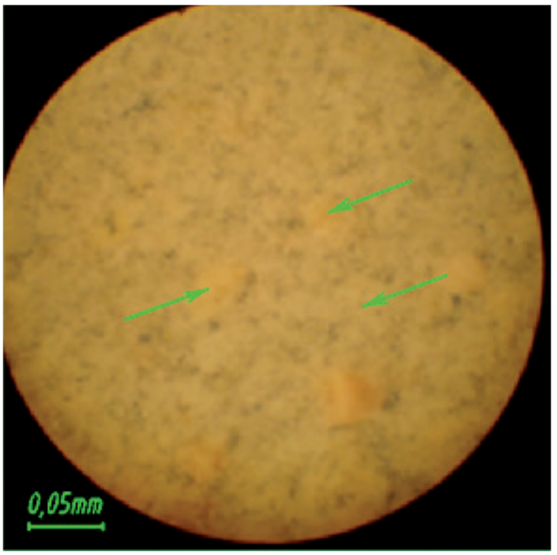

Figure 6: *Treatment with activated sludge, carbamide and air (the scale is 20 × 10).*

55%. Apparently, microorganisms used phosphorus and carbonate carbon in the composition of francolite for their growth and development, which led to a decrease in the grain size. Thus, the particles of phosphorite grains also underwent destruction and from an irregular angular form turned into round ones with a smaller size. Therefore, there is a real possibility of finding out phosphorites and an additional increase in the specific mass of P_2O_5 in the total fertiliser mass.

Analysis of stereoscopic microphotos (Figures 4–6) of calcite crystals showed the presence of calcite minerals in the form of large pieces of opaque colour (indicated by arrows) at the very beginning of the process in the control variant (Figure 4). The size of calcite grains varies from 40 to 80 μm. When calculating the microflora of the active silt (Figure 5), the calcite fragments of the mineral began to disintegrate, and when the microorganisms were fed with carbamide and supplied with oxygen of air (Figure 6), a complete decay of the calcite

occurred, which looked as amorphous in which the calcite grains had a size of less than 1–2 mm. Phosphorite grains in the control variant had a larger size and irregular shape. Depending on the duration of bacterial treatment, the form of phosphorite grains began to decrease (Figures) and take a spherical shape. The main components of phosphorite ores (hardly soluble phosphates) were converted to hydro and dihydrogen phosphates, i.e. into more soluble and digestible forms.

Crystals of calcite began to disintegrate, and under stereoscopic observation using a microscope, they resembled the kind of powdered phosphorite grains (Figures. 4–6).

One of the options for enriching phosphorites, taking into account the grinding of calcite crystals and the change in the dimensions of phosphorite grains, is the possibility of their washing away from each other by a gravitational method. Fine calcites can be separated from larger phosphorite grains.

Among the chemical elements necessary for plants, 16 main biogenic microelements are distinguished: carbon, oxygen, hydrogen, nitrogen; ash elements – phosphorus, potassium, calcium, magnesium and sulphur and trace elements – boron, molybdenum, copper, zinc, cobalt, manganese and iron. The place of one element cannot be replenished by another, because each of them fulfils the specific physiological function assigned to them.

Trace elements are not accidental ingredients of tissues and fluids of living organisms but components of the naturally existing very ancient and complex physiological system involved in regulating the vital functions of organisms at all stages of development. Among the 15 vital elements, nine are cations – calcium (Ca^{2+}), sodium (Na^{+}), potassium (K^{+}), magnesium (Mg^{2+}), manganese (Mn^{2+}), zinc (Zn^{2+}), iron (Fe^{2+}), copper (Cu^{2+}) and cobalt (Co^{2+}). Six others are anions or are contained in complex anionic groups: chloride (Cl^{-}), iodide (J^{-}), phosphate (PO_4^{3-}), sulphate (SO_2^{4-}), molybdate (MoO_2^{3-}) and selenite (SeO_2^{3-}) [5]. Isolations of microorganisms contain a whole complex of organic compounds, consisting of vitamin-like substances and humic, abscisic, gibberellic and other acids in the form of growth stimulators and plant development. Thus, along with the enrichment of low-grade phosphorites with active silt microorganisms and their excreta, they will be enriched by additional stimulating compounds and microelements stimulating growth and development of plants [24].

Conclusion

Treatment of low-grade phosphorites with microflora of activated silt led to a change in the structure of phosphorites, where the destruction of calcite mineral occurred and the phosphorite grains decreased in size and became round in shape, which indicates their partial dissolution and transfer to the form that is assimilated by plants.

Thus, the development of a biotechnological method for the destruction of low-grade phosphorites and their wastes is possible to create not only a fundamentally new technology but also an economically promising technology, since the active sludge is itself a source of macro- and microelements. Applying the methods of gravitational and flotation enrichment, it is possible to separate the maximum amount of calcite from phosphorite grains and supplement it with parallel extraction of radioactive, rare and rare-earth elements.

References

[1] Sultanov, B.E., Tursunova, Z.M., Namazov, S.S., Erkaev, A.U., Beglov, B.M. (2002): Influence of the concentration of a solution of calcium nitrate on the degree of washing of a concentrate of phosphorites of the Central Kyzylkum. *Uzbek chemical journal*, 4, pp. 10–13.

[2] Shilaev, V.P. *Fundamentals of mineral processing*. (1986): Moscow: Nedra, pp. 247–255.

[3] Nabiulina, Y.N., Wasserman, B.I., Panova, N.S. (1977): Reduction of material entrainment during firing" Tr. GIGHS, pp. 92–95.

[4] Cheryatu, Y.S. (1988): Reagents for the flotation of magnesium-containing phosphorite ores. *Dep. In ONIITEHIM*, LGI, p. 6, 1988, 17.10.83.

[5] Malinskaya, I.S. (1968): *Searching for anion collectors for flotation of phosphorites and studying the features of their action*" thesis for Cand. tech. Sci., Moscow, 1968; pp. 85–103.

[6] Chepelevetskiy, M.L., Rubinov, S.S. (1987): Kinetics of the decomposition of minerals of the phosphate complex by acids". *Tr. NIUIF*, 137, pp. 10–73.

[7] Tolstov, E.A., Sytenkov, V.N., Kizimov, F.P. et al. (2002): *Technological instruction for calcination of phosphorite ore from the roasting department*. - Navoiy, NMMC, 2002, pp. 8–26.

[8] Wolfkovich, S.I. (1971): Enrichment of phosphorites of Karatau with sulfuric acid. *Journal applied chemistry*, 5, pp. 969–971.

[9] Orlov, E.A., Treushenko, N.N., Kopylev, B.A., Belchenko, G.V., Pchelintsev, V.N. et al. (1976): On the effect of temperature and composition of the gas and liquid phases on the process of enrichment of Karatau phosphorites with sulfur dioxide. Proceeding of Leningrad Technological Institute Named Lensovet, Leningrad City Council, Issue 5, pp. 137–143.

[10] Treuschenko, N.N., Kopylev, B.A., Belchenko, G.V., Tkacheva, V.A. (1976): Interaction of an aqueous suspension of carbonized phosphorite with nitrogen oxides. Proceeding of Leningrad Technological Institute Named Lensovet, Leningrad City Council, Issue 5, pp. 142–145.

[11] Hill, R.O. (1976): Treatment of materials containing phosphates: The patent of France G 01 in 25/01.-No. 2280584.-Pub. 27.02.76.

[12] Pozhin, M.E., Zhiltsova, D.F., Nikondrov, I.S. (1970): Method for purification of natural phosphorus-containing raw materials from impurities of magnesium compounds. The patent of the USSR Cl. From 05 to 9/00.-No. 283243.- Published on 18.12.70.

[13] Wengeler, W., Volstein, F., Hoffmann, E. (1977): Preparation of phosphate ores (for processing). The patent of Germany Cl. C 01 to 25/22.-No. 2531519.-Published on -20.01.77.

[14] Petersen A.W. (1973): Process of processing phosphate ore. US Patent. Cl. 423–320, C 01 в 25/16.-No. 3717702.-pub.20.02.73.

[15] Kamino, Y. et al. (1982): Preparation of EFC. The patent of Japan. MKI 01 to 25/222.-No. 55–174861.- pub. 23.06.82.

[16] Sardisco, J.B., Holcomb, D.E. et al. (1983): Enrichment of phosphate ponds. US Patent. 4393000 MKI S 01 F 1/00.-No. 338998.-publ.12.07.83.

[17] Rinberg, G.R. et al. (1980): Method for the enrichment of natural phosphates. The patent of the USSR From 05 In 11/04 to 735583. - publ. 25.05.80.

[18] Fedyaeva, O.A., Reshetnikova, E.V., Chachina, S.B. (2012): Investigations of the chemical composition of spent activated sludge of JSC Omsk Vodokanal. Proceedings of OmSTU. Department of Physical Chemistry, Russia, Omsk, p. 8.

[19] Netrouzov, A.I., Bonchosmolovskaya, E.A., Gorlenko, V.M. (2004): *Ecology of microorganisms*. Textbook for students, High schools, Moscow: Academy, pp. 2004–272.

[20] Tepexova, V.F., Burov, I.V. (1982): *Physico-chemical properties and application of rare-earth metals*. GOSINTY.

[21] Mintern, P.A. (1984): New research of rare earth metals. Collection of translations. Ed. EM Savitsky, 2, 212–220. "Mir" Publishing House.

[22] Smirnov, A.I. (1972): *Material composition and conditions for the formation of basic types of phosphorites*. – Moscow, Nedra, p. 196.

[23] Skalny, A.V. (2004): *Chemical elements in human physiology and ecology*. Moscow. ONYX-21 century Mir, p. 218.

[24] Olikulov, F.A., Khamidov, O.Z., Tagayev, I.A. (2016): Development of a method for obtaining bioorganic fertilizers from domestic and industrial wastewater. Academy of Sciences of Uzbekistan. Institute of General and Inorganic Chemistry. Republican Scientific Conference of Young Scientists. Proceedings of the conference High-tech development in production. Tashkent, 2016, pp. 54–55.

Instructions for Authors

RMZ – MATERIALS & GEOENVIRONMENT (RMZ – Materiali in geookolje) is a periodical publication with four issues per year (established in 1952 and renamed to RMZ – M&G in 1998). The main topics are Mining and Geotechnology, Metallurgy and Materials, Geology and Geoenvironment.
RMZ – M&G publishes original scientific articles, review papers, preliminary notes, and professional papers in English. Only professional papers will exceptionally be published in Slovene. In addition, evaluations of other publications (books, monographs, etc.), in memoriam, presentation of a scientific or a professional event, short communications, professional remarks and reviews published in RMZ – M&G can be written in English or Slovene. These contributions should be short and clear.
Authors are responsible for the originality of the presented data, ideas and conclusions, as well as for the correct citation of the data adopted from other sources. The publication in RMZ – M&G obligates the authors not to publish the article anywhere else in the same form.

Specification of the Contributions

Optimal number of pages is 7 to 15; longer articles should be discussed with the Editor-in-Chief prior to submission. All contributions should be written using the ISO 80000.

- Original scientific papers represent unpublished results of original research.
- Review papers summarize previously published scientific, research and/or expertise articles on a new scientific level and can contain other cited sources which are not mainly the result of the author(s).
- Preliminary notes represent preliminary research findings, which should be published rapidly (up to 7 pages).
- Professional papers are the result of technological research achievements, application research results and information on achievements in practice and industry.
- Publication notes contain the author's opinion on newly published books, monographs, textbooks, etc. (up to 2 pages). A figure of the cover page is expected, as well as a short citation of basic data.
- In memoriam (up to 2 pages), a photo is expected.
- Discussion of papers (Comments) where only professional disagreements of the articles published in previous issues of RMZ – M&G can be discussed. Normally the source author(s) reply to the remarks in the same issue.
- Event notes in which descriptions of a scientific or a professional event are given (up to 2 pages).

Review Process

All manuscripts will be supervised shall undergo a review process. The reviewers evaluate the manuscripts and can ask the authors to change particular segments, and propose to the Editor-in-Chief the acceptability of the submitted articles. Authors are requested to identify three reviewers and may also exclude specific individuals from reviewing their manuscript. The Editor-in-Chief has the right to choose other reviewers. The name of the reviewer remains anonymous. The technical corrections will also be done and the authors can be asked to correct the missing items. The final decision on the publication of the manuscript is made by the Editor-in-Chief.

Form of the Manuscript

All papers must be submitted via the online system.
The original file of the Template is available on RMZ – Materials and Geoenvironment Home page address: **www.rmz-mg.com**.

The contribution should be submitted in Microsoft Word. Manuscript should be written in Arial font and 12 pt font with 1.5 line spacing and should contain all figures, tables and formulas. Headings should be written in Arial bold font and shuold not be numbered. Subheadings should be written in Arial italic font. The electronic version should be simple, without complex formatting, hyphenation, and underlining. For highlighting, only bold and italic types should be used.

Annexes

Annexes are images, spreadsheets, tables, and mathematical and chemical formulas. Math formulas should be included in article as editable text and not as images.
Annexes should be included in the text at the appropriate place, and they should also be submitted as a separate document, i.e. separated from the text in the article.
Annexes should be originals, made in an electronic form (Microsoft Excel, Adobe Illustrator, Inkscape, AutoCad, etc.) and in .eps, .tif or .jpg format with a resolution of at least 300 dpi.
The width of the annex should be at least 152 mm. They should be named the same as in the article (Figure 1, Table 1). The text in the annexes should be written in typeface Arial Regular (6 pt).
The title of the image (also schemes, charts and graphs) should be indicated in the description of the image.
When formatting spreadsheets and tables in text editors, tabs, and not spaces, should be used to separate columns.
Each formula should have its number written in round brackets on its right side.
References of the annexes in the text should be as follows: “Figure 1…” and not “as shown below:”. This is due to the fact that for technical reasons the annex cannot always be placed at the exact specific place in the article.

Composition of the Manuscript

Title
The title of the article should be precise, informative and not longer that 100 characters. The author should also indicate the short version of the title. The title should be written in English as well as in Slovene..

Information on the Authors
Information on the authors should include the first and last name of the authors, the address of the institution and the e-mail address of the corresponding author.

Abstract
The abstract presenting the purpose of the article and the main results and conclusions should contain no more than 180 words. It should be written in Slovene and English.

Key words
A list of up to 5 key words (3 to 5) that will be useful for indexing or searching. They should be written in Slovene and English.

Introduction

Materials and methods

Results and discussion

Conclusions

Acknowledgements

References

The references should be cited in the same order as they appear in the article. **Where possible the DOI for the reference should be included at the end of the reference.** They should be numbered in square brackets. References should be cited according SIST ISO 690:1996 standards.

Book:
[1] Reynolds, J.M. (2011). *An introduction to Applied and Environmental Geophysics*. New York: Wiley, 710 p.

Unpublished Master thesis or PhD dissertation:
[2] Trček, B. (2001): *Solute transport monitoring in the unsaturated zone of the karst aquifer by natural tracers*. Ph. D. Thesis. Ljubljana: University of Ljubljana 2001; 125 p.

Chapter in an edited book:
[3] Blindow, N., Eisenburger, D., Illich, B., Petzold, H., Richer, T. (2007): *Ground Penetrating Radar*. In: Environmental Geology: Handbook of Field Methods and Case Studies, Knödel, K., Lange, G., Voigt, H.J. (eds.). Springer: Berlin; pp. 283–335.

Journal article : Journal title should be complete and not abbreviated.
[4] Higashitani, K., Iseri, H., Okuhara, K., Hatade, S. (1995): Magnetic Effects on Zeta Potential and Diffusivity of Nonmagnetic Particles. *Journal of Colloid and Interface Science*, 172, pp. 383–388.
[5] Mcmechan, G.A, Loucks, R.G, Mescher, P.A, Xiaoxian, Z. (2002): Characterization of a coalesced, collapsed paleocave reservoir analog using GPR and well-core data. *Geophysics*, 67, pp. 1148–1158. doi: 10.1190/1.1500376

Proceedings Paper:
[6] Benac, Č., Gržančić, Ž., Šišić, S., Ružić, I. (2008): Submerged Karst Phenomena in the Kvarner Area. In: Proceedings of the 5th International ProGEO Symposium on Conservation of the Geological Heritage, Rab, Croatia, Marjanac, T (ed.). Pro GEO Croatia: Zagreb; pp. 12–13.

Electronic source:
[7] CASREACT – Chemical reactions database [online]. Chemical Abstracts Service, 2000, renewed 2/15/2000 [cited 2/25/2000]. Available on: <http://www.cas.org/casreact.html>.

Scientific articles, review papers, preliminary notes and professional papers are published in English. Only professional papers will exceptionally be published in Slovene.

Units

SI System should be used for units. Physical quantities should be written in Italics (e.g. m, l, v, T). Symbols for units should be in plain text with spaces (e.g. 10 m, 5.2 kg/s, 2 s-1, 50 kPa). All abreviations should be spelt out in full on first appearance.

Manuscript Submission

Please submit your article via RMZ-M&G Editorial Manager System. You can find it on the address:
http://edmgr.editool.com/rmzmag/default.htm

Log in as an author and submit your article.
You can follow the status of your submission in the system manager and your e-mail.

Information on RMZ – M&G

— Assistant editor
  Jože Žarn
  E-mail address: joze.zarn@ntf.uni-lj.si

— Secretary
  Vukič Nivesč
  Telephone: +386 01 47 04 610
  E-mail address: nives.vukic@ntf.uni-lj.si

These instructions are valid from April 2017.